International Journal of Biological Macromolecules 274 (2024) 133163

Contents lists available at ScienceDirect

International Journal of Biological Macromolecules

journal homepage: www.elsevier.com/locate/ijbiomac

Citrullinating enzyme PADI4 and transcriptional repressor RING1B bind in cancer cells

Salome Araujo-Abad [a,b,*,1], Bruno Rizzuti [c,d], Lourdes Soto-Conde [b], Miguel Vidal [e], Olga Abian [d,f,g,h], Adrian Velazquez-Campoy [d,f,g,h], José L. Neira [b,d,**,1], Camino de Juan Romero [b,i,***]

[a] Cancer Research Group, Faculty of Engineering and Applied Sciences, Universidad de Las Américas, 170124 Quito, Ecuador
[b] IDIBE, Universidad Miguel Hernández, 03202 Elche (Alicante), Spain
[c] CNR-NANOTEC, SS Rende (CS), Department of Physics, University of Calabria, 87036 Rende, Italy
[d] Institute of Biocomputation and Physics of Complex Systems (BIFI), Universidad de Zaragoza, 50018 Zaragoza, Spain
[e] Centro de Investigaciones Biológicas Margarita Salas (CSIC), Calle Ramiro de Maeztu, 9, 28040 Madrid, Spain
[f] Instituto de Investigación Sanitaria de Aragón (IIS Aragón), Zaragoza, Spain
[g] Centro de Investigación Biomédica en Red en el Área Temática de Enfermedades Hepáticas y Digestivas (CIBERehd), 28029 Madrid, Spain
[h] Departamento de Bioquímica y Biología Molecular y Celular, Universidad de Zaragoza, 50009 Zaragoza, Spain
[i] Unidad de Investigación, Fundación para el Fomento de la Investigación Sanitaria y Biomédica de la Comunidad Valenciana (FISABIO), Hospital General Universitario de Elche, Camí de l'Almazara 11, 03203 Elche (Alicante), Spain

ARTICLE INFO

Keywords:
Protein-protein interactions
Intrinsically disordered protein
Proximity ligation assay
Isothermal titration calorimetry
Molecular docking
NMR

ABSTRACT

Polycomb groups (PcGs) are transcriptional repressors, formed by a complex of several proteins, involved in multicellular development and cancer epigenetics. One of these proteins is the E3 ubiquitin-protein ligase RING1 (or RING1B), associated with the regulation of transcriptional repression and responsible for monoubiquitylation of the histone H2A. On the other hand, PADI4 is one of the human isoforms of a family of enzymes implicated in the conversion of arginine to citrulline, and it is also involved in the development of glioblastoma, among other types of cancers. In this work, we showed the association of PADI4 and RING1B in the nucleus and cytosol in several cancer cell lines by using immunofluorescence and proximity ligation assays. Furthermore, we demonstrated that binding was hampered in the presence of GSK484, an enzymatic PADI4 inhibitor, suggesting that RING1B could bind to the active site of PADI4, as confirmed by protein-protein docking simulations. *In vitro* and *in silico* findings showed that binding to PADI4 occurred for the isolated fragments corresponding to both the N-terminal (residues 1–221) and C-terminal (residues 228–336) regions of RING1B. Binding to PADI4 was also hampered by GSK484, as shown by isothermal titration calorimetry (ITC) experiments for the sole N-terminal region, and by both NMR and ITC for the C-terminal one. The dissociation constants between PADI4 and any of the two isolated RING1B fragments were in the low micromolar range (~2–10 μM), as measured by fluorescence and ITC. The interaction between RING1B and PADI4 might imply citrullination of the former, leading to several

Abbreviations: ARM, armadillo; BMRB, Biological Magnetic Resonance Bank; C-RING1B, C-terminal region of RING1B (residues 228–336 of the intact protein); CD, circular dichroism; COAD, colon adenocarcinoma; DAPI, 4′6-diamidino-2-phenylindole; GBM, glioblastoma; EGFR, epidermal growth factor receptor; EMT, epithelial-mesenchymal transition; FBS, fetal bovine serum; IDP, intrinsically disordered protein; IF, immunofluorescence; ITC, isothermal titration calorimetry; MM/GBSA, molecular mechanics with generalized Born surface area; PFA, paraformaldehyde; N-RING1B, N-terminal region of RING1B (residues 1–221 of the intact protein); NMR, nuclear magnetic resonance; NUPR1, nuclear protein 1; Pc, Polycomb; PcG, Polycomb group; PBS, phosphate buffer saline; PDAC, pancreatic ductal adenocarcinoma; PLA, proximity ligation assay; PRC, Polycomb Repressive Complex; PTM, post-translational modification; RING, really interesting new gene; RING1B, E3 ubiquitin-protein ligase RING1; RYBP, RING1 and YY1 binding protein; SEM, standard error of the mean; TGFβ, transforming growth factor β; UV, ultraviolet.

* Correspondence to: S. Abad, Cancer Research Group, Faculty of Engineering and Applied Science, Universidad de Las Américas, 170124 Quito, Ecuador.
** Correspondence to: J. Neira, IDIBE, Edificio Torregaitán, Universidad Miguel Hernández, Avda. del Ferrocarril s/n, 03202 Elche (Alicante), Spain.
*** Correspondence to: C. de Juan Romero, Unidad de Investigación, Fundación para el Fomento de la Investigación Sanitaria y Biomédica de la Comunidad Valenciana (FISABIO), Hospital General Universitario de Elche, Camí de l'Almazara 11, 03203 Elche (Alicante), Spain.
E-mail addresses: lourdes.araujo@udla.edu.ec (S. Araujo-Abad), jlneira@umh.es (J.L. Neira), m.juan@umh.es (C. de Juan Romero).
[1] These authors contributed equally to this work.

https://doi.org/10.1016/j.ijbiomac.2024.133163
Received 23 April 2024; Received in revised form 26 May 2024; Accepted 12 June 2024
Available online 13 June 2024

biological consequences, as well as being of potential therapeutic relevance for improving cancer treatment with the generation of new antigens.

1. Introduction

Polycomb proteins arrange to form complexes, the so-called Polycomb Repressive complexes (PRCs), which modify chromatin and implement transcriptional silencing in higher eukaryotes [1,2]. These Polycomb group (PcG) proteins are encoded by genes that act as repressors of the *Hox* genes in Drosophila [3]. The PcG proteins are involved in two main silencing heteromeric complexes called Polycomb repressive complex 1 and 2 (PRC1 and PRC2); moreover, PRC1 and PRC can work to silence genes either in isolation or synergistically [4,5]. The dysregulation of both complexes is related very often with the onset of cancer or developmental disorders [6–8]. PRC1 and PRC2 are known to be crucial for both the control of carcinogenesis and the self-renewal of stem cells [9]. In mammals, the PRC2 core is formed by at least four heteromeric units, one of which is EZH2 (or its paralogue, EZH1), the methyltransferase that catalyzes the trimethylation of histone H3 at Lys27 [5]. This modification can act as an anchoring site of PRC1 complexes containing chromobox (CBX) proteins. These CBX proteins recruit PRC1 complex onto PRC2-enriched chromatin, easing their monoubiquitylation. The PRC1-dependent monoubiquitylation at Lys119 of histone H2A correlates with transcriptional repression [10–13]. This process is carried out by a heterodimeric RING finger E3 ligase, whose subunit binding is RING1B (also known as RFN2 or RING2), or its paralogue RING1A. The 334-residue-long RING1B is involved in the development and progression of several human cancers [14–17], especially human hepatocellular and pancreatic ones [18]. In hepatocellular and colorectal carcinomas, RING1B is a negative regulator of p53 homeostasis, and it interacts with and ubiquitinates p53 causing its proteasome degradation. In cancer cells with wild-type p53, the lack of RING1B inhibited the proliferation of the cells by inducing cell-cycle arrest, apoptosis, and senescence [19]. RING1B upregulation is positively correlated with radio-resistance in lung cancer and chemoresistance in ovarian cancer, as well as with the incidence and progression of hepatocellular carcinoma, melanoma, prostate cancer, breast cancer, pancreatic cancer, gastric cancer, and bladder urothelial carcinoma [20].

The RING finger proteins [21] have a so-called RING motif [22]. They often form homodimeric or heterodimeric pairs [23,24], through the binding of the N-terminal RING region of each monomer. We have previously described the conformational properties of the dimeric C-terminal domain of RING1B (C-RING1B), the so-called RAWUL one, encompassing the residues 228–336 [25]. The X-ray structure of the monomers of C-RING1B resembles that of a ubiquitin module, and it serves to interact with CBX proteins [26]. Furthermore, we have also shown that C-RING1B can interact with: (i) RING1 and YY1 binding protein (RYBP) [27,28], which is a highly basic, intrinsically disordered protein (IDP) and a non-canonical component of the PRC1 [12,29–31]; (ii) nuclear protein 1 (NUPR1), another basic IDP [32]; and (iii) NUPR1L, the paralogue of NUPR1, which is also a basic IDP [33], and therefore,C-RING1B could be involved in the binding to other protein partners, acting as a modulator of several of them. We have also characterized the structural and conformational properties of the N-terminal region of RING1B (N-RING1B), a fragment comprising the first 221 residues of RING1B [34]. This fragment contains the 41-residue-long RING finger motif, and flanking sequences that form an interacting polypeptide patch for PcG and non-PcG proteins. The N-Ring1B fragment is monomer, with evidence of having a native-like structure [34]. Furthermore, isolated N-Ring1B binds to the E2 ubiquitin conjugase of *Carassius auratus* – as the intact RING1B does, after forming previously a binary complex with a completely different protein – and to UbcH5c, which is the E2 protein belonging to the ubiquitin conjugation pathway [35].

PADI4 is a member of the family of peptidyl-arginine deiminases, in charge of catalyzing citrullination, *i.e.*, the conversion of arginine to citrulline residues in a polypeptide chain, in the presence of Ca(II) ions. Unless the substrate protein is degraded, this post-translational modification (PTM) is permanent. Such PTM alters the molecular properties of the affected polypeptide chain, and it has important roles in human diseases [36–39]. PADI4 is usually located, among other places, in the cytoplasmic granules of eosinophils, neutrophils or macrophages; and in tumor cells, where it is highly expressed, either in the cytosol or in the nucleus. PADI4 is involved in gene transcription and immune system modulation [40–44]; furthermore, an increase in the citrullinating activity is observed for several PADI4 haplotype mutants during apoptosis enhanced through the mitochondrial pathway [45]. In addition, PADI4 is involved in p53 gene expression, as well as in the expression of other p53-target genes [44,46,47]. We have recently shown that PADI4 is expressed in glioblastoma (GBM), pancreatic adenocarcinoma (PDAC) and colon cancer [48], and it binds to other key proteins involved in cancer development, such as importin α3 [49], plakophilin 1 [50], murine double minute 2, MDM2, [51], NUPR1 [52], and RYBP [53]. Therefore, provided the protein partners in common between RING1B and PADI4, and their similar expression in tumor cells, we hypothesized that they could also bind directly to each other.

In this work, we provided evidence for the association between each of the two fragments of RING1B, N-RING1B and C-RING1B, to PADI4. With such "divide-and-conquer" approach, we showed that binding to RING1B by PADI4 may occur at different places of the polypeptide chain, and not only in correspondence with the well-folded C-RING1B domain. Binding to both fragments was tested *in vitro* by using several spectroscopic and biophysical techniques, and it occurred with affinities in the low micromolar range. These results were also confirmed by *in silico* experiments. Binding was also tested *in cellulo* by using immunofluorescence (IF) and proximity ligation assay (PLA) in different cancer cells, and it was hampered by using GSK484, an enzyme inhibitor of PADI4. Those results indicate that the RING1B-binding region of PADI4 could be close to its active site or, alternatively, in another region associated with an allosteric inhibition. The fact that RING1B interacts directly with PADI4, and it may undergo citrullination, opens new scenarios in the biological pathways it is involved into.

2. Materials and methods

2.1. Materials

Imidazole, Trizma base and acid, DNase, SIGMAFAST protease tablets, NaCl, Ni(II)-resin, anti-RING1B antibody, DAPI (4′,6-diamidino-2-phenylindole) and ultra-pure dioxane were from Sigma (Madrid, Spain). Ampicillin, kanamycin and isopropyl-β-D-1-thiogalactopyranoside were obtained from Apollo Scientific (Stockport, UK). Dialysis tubing with a molecular weight cut-off of 3500 Da, Triton X-100, TCEP (tris(2-carboxyethyl)phosphine), glycerol and the SDS protein marker (PAGEmark Tricolor) were from VWR (Barcelona, Spain). Amicon centrifugal devices with a molecular weight cut-off of 30 kDa were from Millipore (Barcelona, Spain). The rest of the materials were of analytical grade. Water was deionized and purified on a Millipore system.

2.2. Protein expression and purification

The dimeric protein PADI4 (with 663 residues *per* monomer), the dimeric C-RING1B and monomeric N-RING1B were purified as previously described [25,34,48]. For the ^{15}N-labeled His-tagged C-RING1B,

BL21 cells were grown in M9 minimal medium supplemented with 1 g of $^{15}NH_4Cl$ *per* liter of media, and the protein was purified by using the same protocol as that followed in Luria-Bertani media [25].

Protein concentrations were determined by UV absorbance, employing an extinction coefficient at 280 nm estimated from the number of tyrosines and tryptophans in each protein [54]: PADI4 has 10 tryptophans and 13 tyrosines *per* monomer; C-RING1B has 1 tryptophan and 7 tyrosines *per* monomer; and N-RING1B has 1 tryptophan and 3 tyrosines.

2.3. Cell lines

Isolation of the primary human GBM cell line HGUE-GB-42 was performed from surgical washes, as reported previously [55]. Human pancreatic adenocarcinoma (RWP-1) and colorectal cancer (SW-480) cell lines were donated by Instituto Municipal de Investigaciones Médicas (IMIM, Barcelona, Spain) [56]. The RWP-1 and SW-480 cell lines were cultured in Dulbecco's Modified Eagle's Medium: High Glucose (DEMEM-HG) (Biowest, MO, USA). GBM cells were cultured in Dulbecco's Modified Eagle's Medium: Nutrient Mixture F-12 (DMEM F-12) (Biowest, MO, USA). Both media were supplemented with 10 % (*v*/v) heat-inactivated fetal bovine serum (FBS) (Capricorn Scientific, Ebsdorfergrund, Germany) and 1 % (v/v) penicillin/streptomycin mixture (Biowest, MO, USA). Cells were incubated at 37 °C in a humidified 5 % CO_2 atmosphere as previously described [57].

2.4. Immunofluorescence (IF)

An amount of 30,000 cells from HGUE-GB-42, SW-480, and RWP-1 cell lines were seeded into twenty-four-well plates on coverslips. After 24 h, they were fixed with paraformaldehyde (PFA) at 4 % concentration and blocked with FBS/PBS (1×) (50 μL/mL). Next, cells were incubated with anti-PADI4 (1:200, mouse; Abcam, Cambridge, UK) and anti-RING1B (1:100, rabbit; Abcam, Cambridge, UK) antibodies.

After washing out the first antibody, cells were incubated with Alexa Fluor 568-labeled anti-mouse (1:500) and Alexa Fluor 488-labeled anti-rabbit (1:500) secondary antibodies (Invitrogen, Barcelona, Spain); the DAPI reagent was used to stain the nucleus. Coverslips were mounted in Prolong™ Gold Antifade Reagent (Invitrogen, Barcelona, Spain) and analyzed using a confocal LSM900 with Airyscan 2 microscope (Carl Zeiss, Oberkochen, Germany) at ×63 magnification.

2.5. Proximity ligation assay (PLA)

An amount of 30,000 cells of HGUE-GB-42, SW480 and RWP-1 cell lines were seeded in twenty-four-well plates on coverslips. After 24 h, cells were washed in PBS (1×), fixed with PFA 4 %, washed again, permeabilized in PBS (1×) with 0.2 % Triton X-100, and blocked with blocking solution for 1 h at 37 °C before immune-staining with DuoLink by using PLA Technology (Merck, Madrid, Spain), following the manufacturer's protocol. Anti-PADI4 and anti-RING1B primary antibodies were used. Then, slides were processed for *in situ* PLA by using sequentially the DuoLink *In Situ* PLA Probe Anti-Mouse MINUS, DuoLink *In Situ* PLA Probe Anti-Rabbit PLUS, and DuoLink *In Situ* Detection Reagents Red (Merck, Madrid, Spain). In these experiments, red fluorescence spots correspond to the PLA-positive signals, indicating that the two proteins are bound, forming a protein complex; on the other hand, the blue fluorescence spots correspond to nuclei (DAPI staining). Both negative and positive control experiments were performed, the former by omitting one of the primary antibodies. Image acquisition was carried out by using a confocal microscope LSM900 with Airyscan 2 (Carl Zeiss, Oberkochen, Germany) at × 63 magnification.

In PLAs with the presence of GSK484, cells were previously subjected to treatment with 20 μM of GSK484 for either 6 or 24 h.

2.6. Statistical analyses of in cellulo experiments

The number of red dots was counted by using the Fiji software (Image J2). The results are given as the mean ± standard error of the mean (SEM) of three independent experiments ($n = 5$ images). To evaluate the normal distribution of the data, the Shapiro–Wilk statistical test was used. Subsequently, we employed a 1-way ANOVA, Tukey's *post hoc* test to analyze the association between variables. Differences were considered statistically significant with a p-value <0.05. Statistical analysis was performed with GraphPad Prism v7.0a software (GraphPad Software Inc., San Diego, CA, USA).

2.7. Fluorescence

2.7.1. Steady-state fluorescence

A Cary Varian spectrofluorometer (Agilent, Santa Clara, CA, USA), interfaced with a Peltier unit, was used to collect fluorescence spectra at 25 °C by excitation at either 280 or 295 nm; slit widths were 5 nm. The other experimental parameters have been described elsewhere [58]. Appropriate blank corrections were made in all spectra. Following the standard protocols used in our laboratories, the samples were prepared the day before and left overnight at 5 °C; before experiments, samples were left for 1 h at 25 °C. A 1-cm-path length quartz cell (Hellma, Kruibeke, Belgium) was used. For the experiments with each RING1B fragment, the final PADI4 protein concentration was 2 μM (in protomer units). The corresponding concentration of the RING1B fragment, either N-RING1B or C-RING1B, was 20 μM. Experiments were performed in 20 mM Tris buffer (pH 7.5), 5 mM TCEP, 10 mM EDTA, 150 mM NaCl and 5 % glycerol, in triplicates with newly prepared samples. Variations of results among the experiments were lower than 5 %.

2.7.2. Fluorescence binding experiments with the RING1B fragments and PADI4

For the titration between each RING1B fragment and PADI4, increasing amounts of the corresponding fragment species, in the concentration range 0–30 μM (final protomer concentration), were added to a solution with a fixed concentration of PADI4 (2.0 μM in protomer units). The samples were prepared the day before and left overnight at 5 °C; before the measurements, they were incubated for 1 h at 25 °C. Experiments were carried out in the same buffer used for the steady-state experiments. The samples were excited at either 280 or 295 nm, and the rest of the experimental set-up was the same described above. In all cases, the appropriate blank-corrections were made by subtracting the signal obtained with the corresponding amounts of the RING1B fragment (both hereafters indicated indistinctly as X-RING1B) by using the software KaleidaGraph (Synergy software, Reading, PA, USA). Spectra were corrected for inner-filter effects during fluorescence excitation [59]. The titration was repeated three times, using new samples; variations in the results were lower than 10 %.

The dissociation constant of the corresponding complex, K_d, was calculated by fitting the binding isotherm constructed by plotting the observed fluorescence change as a function of concentration of the X-RING1B fragment to the general binding model, explicitly considering protein depletion due to binding [60,61]:

$$F = F_0 + \frac{\Delta F_{max}}{2[PADI4]_T}\left([\mathrm{X-RING1B}]_T + [PADI4]_T + K_d\right) - \sqrt{\left(\left([\mathrm{X-RING1B}]_T + [PADI4]_T + K_d\right)^2 - 4[\mathrm{X-RING1B}]_T[PADI4]_T\right)}, \quad (1)$$

where F is the measured fluorescence of the solution with the fixed PADI4 concentration (2.0 μM, in protomer units) and that of X-RING1B (*i.e.*, either RING1B fragment), after subtraction of the corresponding blank with the same concentration of the fragment; ΔF_{max} is the largest change in the fluorescence of X-RING1B when all polypeptide molecules

were forming the complex, compared to the fluorescence of each isolated chain; F_0 is the fluorescence intensity when no X-RING1B was added; $[PADI4]_T$ is the constant, total concentration of PADI4 (2.0 μM); and $[X\text{-}RING1B]_T$ is that of each X-RING1B, which was varied during the titration. Fitting of data to the above equation was carried out by using KaleidaGraph (Synergy software, Reading, PA, USA).

2.8. Circular dichroism (CD)

Far-UV CD spectra were collected on a Jasco J810 spectropolarimeter (Jasco, Tokyo, Japan) with a thermostated cell holder and interfaced with a Peltier unit. The instrument was periodically calibrated with (+)-10-camphorsulfonic acid. A 0.1-cm path length quartz cell was used (Hellma, Kruibeke, Belgium). All spectra were corrected by subtracting the corresponding baseline. Concentration of each polypeptide (PADI4 and the corresponding X-RING1B) and the buffers were the same used for fluorescence experiments. Samples were prepared the day before and left overnight at 5 °C to allow them to equilibrate. Before starting the experiments, samples were further left for 1 h at 25 °C. Isothermal wavelength spectra of each isolated macromolecule and those of the complex were acquired as an average of 6 scans, at a scan speed of 50 nm/min, with a response time of 2 s and a band-width of 1 nm.

Thermal scans of each isolated fragment and that of the corresponding complex were carried out by following the raw ellipticity at 222 nm, with a scan speed of 60 °C/h, a response of 8 s, a band width of 1 nm, and a data pitch of 0.2 °C. Raw ellipticity was collected between 25 and 85 °C.

The thermal denaturations were irreversible in all complexes formed between PADI4 and either X-RING1B fragment; nevertheless, we obtained an apparent thermal denaturation midpoint, T_m, allowing a qualitative estimate of the complex formation: if the complex was formed, we should observe an increment in the T_m when compared to that calculated from the thermal denaturation of the isolated X-RING1B. The change in the raw ellipticity at 222 nm, Θ, was fitted to:

$$\theta = \left(\theta_N + \theta_D e^{(-\Delta G/RT)}\right) / \left(1 + e^{(-\Delta G/RT)}\right), \quad (2)$$

where ΔG is the change in free energy, when the polypeptide chain or the complex were unfolded; R is the gas constant; and T is the temperature. The ΔG was given by:

$$\Delta G = \Delta H_m(1 - T/T_m) - \Delta C_p[(T_m - T) + T\ln(T/T_m)], \quad (3)$$

where ΔH_m is the van't Hoff unfolding enthalpy; and ΔC_p is the heat capacity change during the unfolding reaction. The form of Eq. (2) does not impose restrictions on the value of the ΔC_p in Eq. (3) used in the fitting.

2.9. Nuclear magnetic resonance (NMR)

The NMR experiments were run at 25 °C on a Bruker Avance DRX-500 spectrometer (Karlsruhe, Germany) equipped with a triple resonance probe and z-pulse field gradients. Spectra were acquired at 25 °C in 20 mM Tris buffer (pH 7.5), 5 mM TCEP, 150 mM NaCl, 10 mM EDTA, and 5 % glycerol with 50 μL of D_2O; probe temperature was calibrated with a methanol NMR standard [62].

Three different 2D ^{1}H-^{15}N HSQC NMR spectra [63] were obtained on samples containing: (i) isolated C-RING1B (90 μM of final concentration in protomer units); (ii) C-RING1B (90 μM of final concentration in protomer units) in the presence of 340 μM of PADI4 (final concentration in protomer units); and (iii) C-RING1B (90 μM of final concentration in protomer units) in the presence of 340 μM of PADI4 (final concentration in protomer units) and 340 μM of GSK484. All spectra were acquired in TPPI mode at 25 °C with 2048 complex points in the ^{1}H dimension, 200 complex points in the ^{15}N dimension, with 192 scans. Typical spectral widths for the 2D ^{1}H-^{15}N HSQC spectra were 6000 (^{1}H) and 1500 (^{15}N) Hz. Water was removed by using the WATERGATE sequence [64].

The sample containing the mixture of PADI4 and C-RING1B was prepared by using Amicon centrifugal devices of 3 kDa cut-off, in which both proteins were initially mixed at diluted concentrations in the above indicated buffer, and then concentrated in the same buffer; any possible precipitation product observed in the Amicon device was removed during the concentration step. For the experiments in the presence of GSK484, after the concentration step, a corresponding volume of a concentrated stock solution of the inhibitor was added to the solution of the complex. In both cases (either in the presence or absence of GSK484), at the end of the concentration step when the final volume of the concentrated solution was 400 μL, 50 μL of D_2O and the same volume of a concentrated (10×) stock solution of the above buffer were added. The pH of the three samples (complex PADI4/C-RING1B without GSK484; complex PADI4/C-RING1B with GSK484; and isolated C-RING1B) was measured after removal from the Amicon device with an ultra-thin electrode. Values of the pH reported here represent apparent values of pH, without correction for isotope effects. The methyl protons of TSP were used as the internal chemical shift reference for ^{1}H and for the indirect ^{15}N dimension and they were corrected for the pH value [62] in all spectra. It is important to stress that no assignment of C-RING1B is available in the Biological Magnetic Resonance Bank (BMRB), and therefore the HSQC spectra were used as qualitative indicators of change occurring in the presence of PADI4. All spectra were processed with TopSpin 2.1 (Bruker, Karlsruhe, Germany).

2.10. Isothermal titration calorimetry (ITC)

The interaction of PADI4 with C-RING1B and N-RING1B was assessed by using an Auto-iTC200 automated high-sensitivity calorimeter (MicroCal, Malvern-Panalytical, Malvern, UK). Calorimetric titrations were performed at 25 °C in 20 mM Tris, at pH 7.5. Either C-RING1B or N-RING1B (~90–100 μM) in the injection syringe was titrated into the PADI4 solution (8 μM) in the calorimetric cell. Experiments with both fragments in the presence of GSK484 were carried out by adding a final 100 μM concentration of such compound to PADI4 in the calorimetric cell.

A series of 19 injections with 2 μL volume, at 0.5 μL/s injection speed, and 150 s time spacing was programmed while maintaining a reference power of 10 μcal/s and a stirring speed of 750 rpm. Integration of the thermal power raw data was used to calculate the heat effect *per* injection. The interaction isotherm, which is the ligand-normalized heat effect *per* injection as a function of the molar ratio, was analyzed by non-linear least squares regression data analysis. A model considering a single binding site was used to estimate the association constant, K_a; the interaction enthalpy, ΔH; and the apparent stoichiometry of binding, n, although, in practice, the latter is usually interpreted as the fraction of active protein in the cell/syringe. The Gibbs energy of interaction, $-\Delta G$, and the entropic contribution, $-T\Delta S$, were calculated according to well-known thermodynamic relationships: $\Delta G = -RT\ln K_a$ and $\Delta G = \Delta H - T\Delta S$. The background injection heat was accounted for by including an adjustable constant parameter in the fit. The data analyses were conducted in Origin 7.0 (OriginLab, Northampton, MA, USA) with user-defined fitting functions.

2.11. Protein-protein molecular docking

Protein-protein docking was used to determine the structure of the complex between the two proteins. PADI4 was modeled in its homodimeric structure, on the basis of its crystallographic structure, as previously described [51], with each monomer encompassing 663 residues. The structure of RING1B (entry corresponding to the UniProt identifier Q99496) was obtained from the AlphaFold predictor [65] and included a total of 336 residues. The N-terminal fragment N-RING1B was modeled as having a significantly shorter length (residues 1–134) compared to the construct used in our wet lab experiments (residues

1–221) because the sequence segment 135–221 was a predicted by AlphaFold to be very mobile, as it was formed by an unanchored α-helix followed by a very long (67 residues) completely disordered region.

Docking simulations of PADI4 (considered as host) and the two fragments N-RING1B or C-RING1B (each considered as a guest in the molecular complex) were performed in a blind fashion, without any assumption on the possible binding interface for any of the protein species. ClusPro [66] and several other algorithms available in public web servers [67] were used, in all cases with their default simulation parameters. Their best predictions were compared by re-ranking them on the basis of calculations performed using molecular mechanics with the generalized Born surface area (MM/GBSA) methodology [68] using the HawkDock web server [69]. However, when the computational results were rigorously screened against the other findings we obtained with our wet-laboratory techniques, the docking predictions of ClusPro were the sole consistent with the experiments.

3. Results

3.1. Intact RING1B and PADI4 interacted in cellulo both in the cytoplasm and the nucleus

To test whether the interaction between endogenous PADI4 and intact RING1B occurred within cancer cells, we used different cell lines. For GBM, we employed a previously described patient-derived cell line, HGUE-GB-42, from now on GB-42 [55]. We also used other two cell lines: SW-480, isolated from the large intestine of a Dukes C colorectal cancer patient; and RWP-1, a model of pancreatic cancer. First, we performed IF experiments to address whether both proteins were expressed and colocalized in the same cellular compartments for the different cell lines (Figs. S1 and S2). We observed that PADI4 was highly expressed in the nucleus of GBM and colon adenocarcinoma (COAD), as shown by the colocalization with DAPI, but mostly in the cytoplasm in the pancreatic tumor cell, in accordance with previous observations [48]. RING1B was expressed in the cytoplasm and nucleus depending on

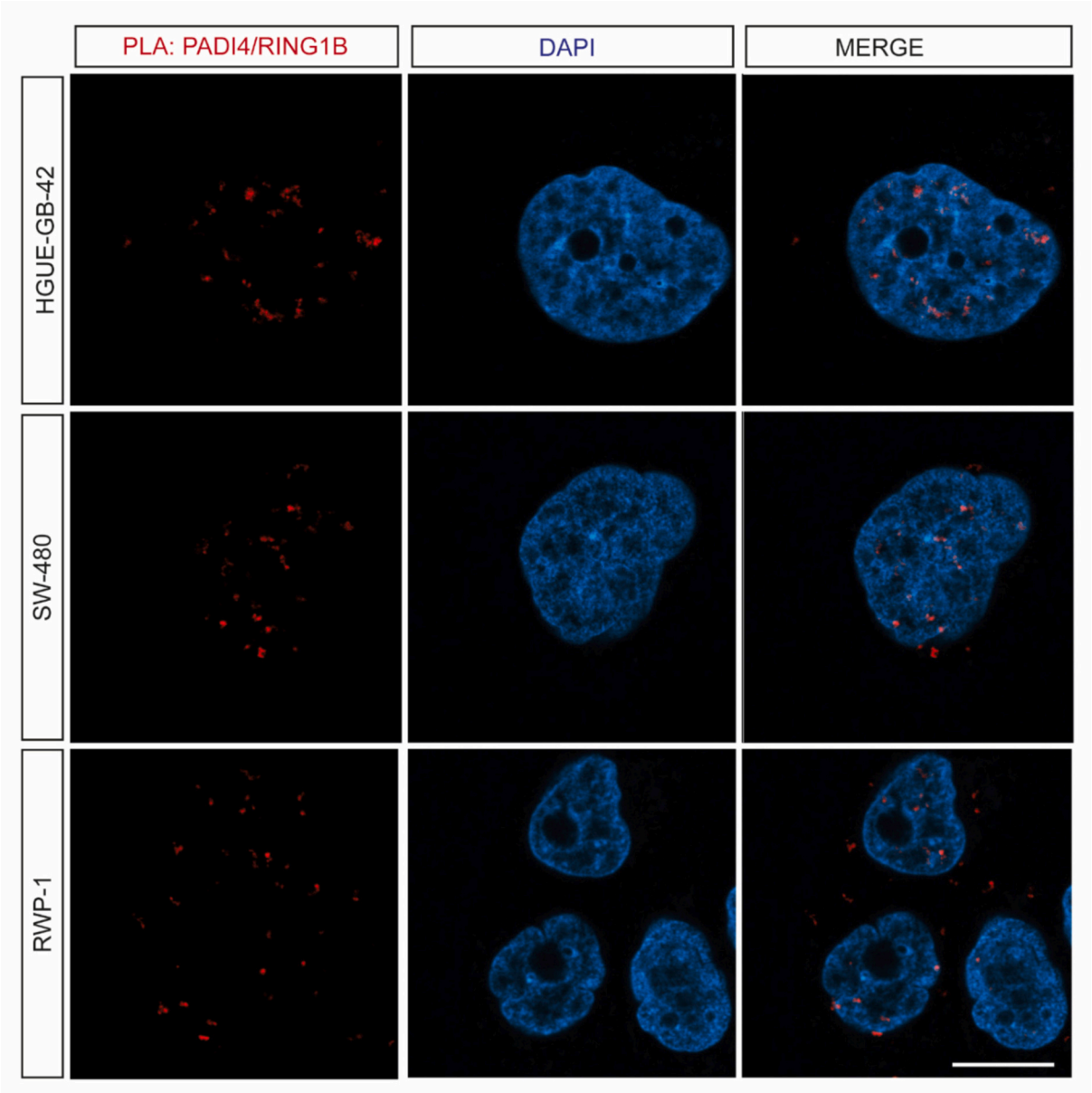

Fig. 1. RING1B binding to PADI4 *in cellulo*. PLAs of PADI4 with RING1B reveal the interaction between the two proteins in different patient-derived cells. A representative experiment is shown (n = 5). Scale bar = 10 μm.

the tumor cell line, and similarly to PADI4 it was mostly cytoplasmatic in RWP-1. The different expression patterns of PADI4 suggested that it may interact with RING1B in diverse cell compartments, depending on the cell line. Therefore, we studied the *in cellulo* interaction after 24 h of the two proteins by using the DuoLink *in situ* assay (PLA).

The red fluorescent spots, corresponding to the PLA signals, indicated that PADI4 interacted with RING1B within the nucleus and cytosol in all tumor cell lines. In accordance with IF experiments, the interaction was mainly in the nucleus of GBM and colon cancer cell lines while it was in the cytoplasmatic compartment in pancreatic cancer (Figs. 1, S3). This observation incontrovertibly demonstrates a direct association of the two proteins within a cellular context, and under the relatively different conditions that such diverse cell types undergo.

To sum up, our results indicate that PADI4 and intact RING1B not only co-expressed, but they interacted in different cell compartments of cancer cells corresponding to several tissues.

3.2. Enzymatic inhibition of PADI4 in cellulo hindered the PADI4/RING1B interaction

The compound GSK484 has been described as an enzymatic inhibitor of PADI proteins, and it shows a strong preference for PADI4 over the other isozymes [70]. Building on our previous experience on the use of GSK484 with the cell lines described above [51], we performed a series of PLAs at 20 μM concentration of GSK484 with PADI4 and RING1B.

We treated all the previously used tumor cell lines with GSK484 for 6 and 24 h, and afterwards we immobilized them after 48 h to perform PLAs. After 6 h, GB-42 and RWP-1 presented a great reduction in the number of observed red dots as compared with SW-480 (Figs. 2A and S4). PADI4/RING1B interaction was equally located in the nucleus and cytoplasm in SW-480 whereas in the other two tumor cell lines, they were mostly nuclear. Along this line, the effect of GSK 484 was affecting mostly the binding in the nucleus in those cell lines, which explained the fact that GB-42 and RWP-1 were the cell lines showing the greater effect after 6 h of treatment (Fig. 2B).

After 24 h of GSK484 treatment, there was an overall decreased in the total number of interactions in all studied cell lines (Fig. 2). Interestingly, this reduction was mostly due to a decrease in the number of interactions in the cytoplasm of SW-480 and RWP-1 when compared to the 6 h treatment. On the other hand, the number of cytoplasm interactions in GBM remained unchanged, whereas nuclear interactions continued to decrease (Fig. 2B).

Altogether our results showed a very strong reduction in the population of PADI4/RING1B formed complexes after the 6-hour treatment with the inhibitor and even greater after 24 h, abolishing almost completely the interaction in all the tumor cell lines (Figs. 2, S4). Therefore, those results indicate that the binding of GSK484 could prevent the association of the two proteins. Remarkably, we observed that the PADI4/RING1B interaction decreased in each cellular compartment and it was different among the tumor cell lines. This was in agreement with previous observations reporting that PADI4 inhibition results in different outcomes in multiple cancer cell lines [36], besides the different enzyme expression among several cancer cell types, as we have recently shown [48]. These overall findings further support the

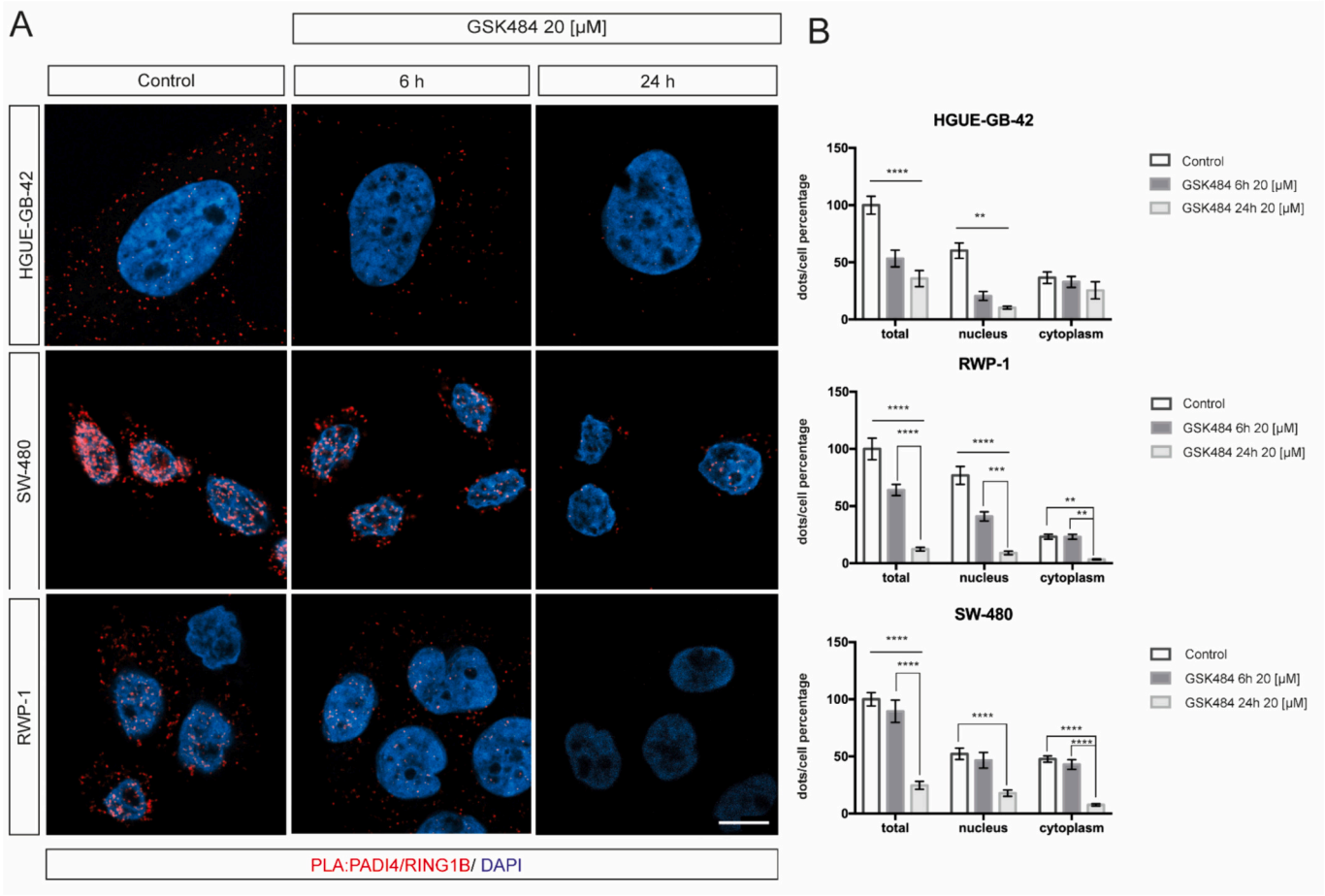

Fig. 2. Inhibition of the formation of the PADI4/RING1B complex by the presence of GSK484 *in cellulo*. (A) PLA performed in HGUE-GB-42 and SW-480 cells in the absence or presence of GSK484 at a concentration of 20 μM, for 6 and 24 h. A representative experiment is shown ($n = 5$). (B) The Fiji software was used to account for the number of red dots. Scale bar = 10 μm. Data represent mean ± SEM, 1-way ANOVA, Tukey's *post hoc* test was used, $^{*}p < 0.05$, $^{**}p < 0.01$, $^{***}p < 0.001$; $^{****}p < 0.0001$. (For interpretation of the references to colour in this figure legend, the reader is referred to the web version of this article.)

inhibitory effect of GSK484 may have different outcomes among the cell lines [71–74].

Altogether, our *in cellulo* experiments showed that, in the presence of GSK484, the binding between RING1B and PADI4 was hampered in all tested tumor cell lines.

3.3. Measuring the affinity of RING1B and PADI4 in vitro

As we had previously shown that there was binding between the two intact proteins *in cellulo*, next we wanted to measure quantitatively such interaction *in vitro*. To define precisely which region of RING1B interacted with PADI4, we used the two different fragments of RING1B: N-RING1B, comprising residues 1–221, which contains native-like folded structure [25]; and C-RING1B, comprising residues 228–336, which is mostly well-folded with a ubiquitin-like domain [34]. In this way, it would be easier to identify possible binding regions in each of the two fragments.

We followed a three-part experimental approach. First, we used steady-state fluorescence and CD, as spectroscopic techniques capable of detecting possible binding and concomitant conformational changes in any of the macromolecules. Second, we used fluorescence titration to measure the affinity of each of the two fragments with PADI4. And finally, we used ITC to quantitatively measure the thermodynamic parameters for the binding of each fragment to PADI4.

3.3.1. Affinity of the N-terminal region (N-RING1B) to PADI4

We used steady-state fluorescence to determine whether there was a change in: (i) the value of the maximum wavelength in the emission spectrum; (ii) the fluorescence intensity observed at that maximum wavelength; or (iii) both the physical parameters, when the spectrum of the complex between PADI4 and N-RING1B was compared to that obtained from the addition of those of the two isolated polypeptide chains.

A variation in fluorescence intensity by excitation at 280 nm was observed when the complex of N-RING1B with PADI4 was formed (Fig. 3A), but there were no changes in the maximum wavelength of the spectrum. Similar variations were observed by excitation at 295 nm. These findings indicate that the tertiary structure around some of the aromatic residues of at least one of the two polypeptide chains changed upon complex formation.

Next, we carried out far-UV CD measurements, with the aim of further supporting the results obtained by fluorescence. The far-UV addition spectrum was different to that of the complex (Fig. 3B). The differences could be either attributed to a relatively large number of aromatic residues involved in the binding, or even to changes in the conformation of both proteins when they are bound. In the latter case, since N-RING1B is partially disordered [34] and PADI4 is well-folded, it would be much more likely that the conformational propensities of N-RING1B were altered upon binding.

We also carried out thermal denaturations followed by far-UV CD. Since the PADI4 concentration was very low (2 μM), the influence of its unfolding in the thermogram should be very small. The rationale behind the use of thermograms to monitor the binding is based on the fact that, if there is binding between the two polypeptide chains, then the thermal denaturation midpoint of the complex should be greater than those of the two isolated polypeptide chains. We observed that the thermal denaturation midpoint of N-RING1B increased from 47.6 ± 0.3 °C (320.6 ± 0.3 K) to 51.5 ± 0.2 °C (320.6 ± 0.2 K, and in both cases, we observed a single sigmoidal transition (Fig. 3C).

Finally, we carried out fluorescence titrations to quantitatively measure the binding affinity of the two polypeptide chains, by keeping constant the concentration of PADI4 and increasing the concentration of N-RING1B. The results indicate (Fig. 4A) that the dissociation constant, K_d, was 9 ± 2 μM. We also used Job's plot to characterize the binding of these proteins, following standard procedures described previously in the literature [75–77]. The intersection concentration value of the two lines relative to the rate of the concentrations of the two proteins species

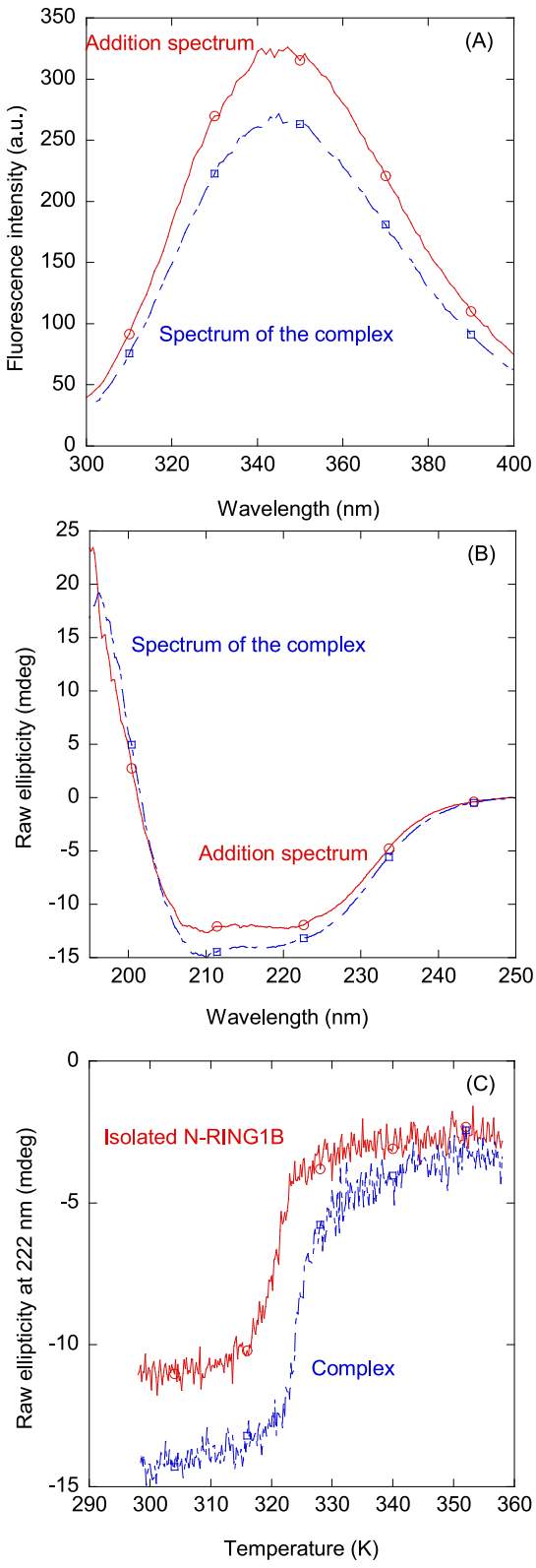

Fig. 3. Binding of N-RING1B to PADI4 as monitored by spectroscopic techniques: (A) Fluorescence spectrum obtained by excitation at 280 nm of the PADI4/N-RING1B complex, and addition spectrum obtained by the sum of the spectra of the two isolated macromolecules. (B) Far-UV CD spectrum of the PADI4/N-RING1B complex, and addition spectrum obtained by the sum of the spectra of the two isolated macromolecules. All experiments were performed at 25 °C. (C) Thermal denaturation scans of isolated N-RING1B and the complex N- PADI4/N-RING1B followed by far-UV CD.

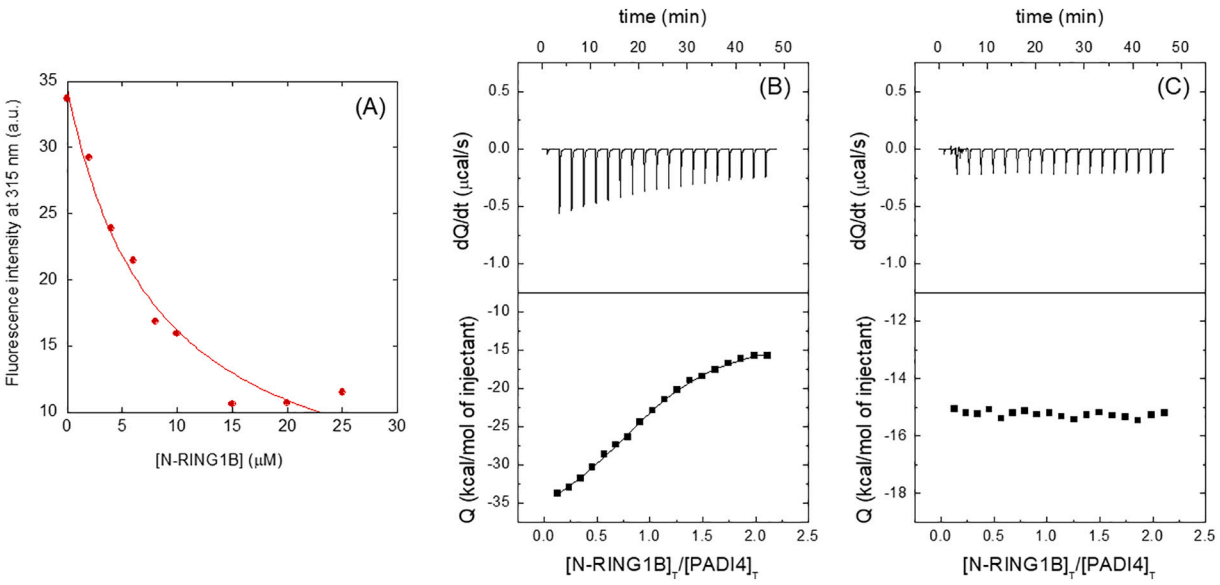

Fig. 4. Quantitative determination of the binding of N-RING1B to PADI4 as monitored by biophysical techniques: (A) Titration curve monitoring the changes in the fluorescence at 330 nm when N-RING1B was added to PADI4. The fluorescence intensity is the relative signal after removal of the corresponding blank. The line through the data is the fitting to Eq. (1). Calorimetric titrations for N-RING1B binding to PADI4 in the absence (B) and presence (C) of GSK484. Upper panels show the thermograms (thermal power as a function of time) and lower panels show the binding isotherms (ligand-normalized heat effects *per* injection as a function of the molar ratio in the calorimetric cell). Continuous lines correspond to the fitting curves according to an interaction model with a single ligand binding site. All experiments were carried out at 25 °C.

(Fig. S5 A) corresponds to the value 2.3, which is an estimate of the concentration rate [N-RING1B]/[PADI4$_{protomer}$]. We also used ITC to determine the thermodynamic binding parameters, *i.e.*, the enthalpy and the entropy of the binding reaction (Fig. 4B). According to the calorimetric experiments, the dissociation constant, K_d, for the interaction of PADI4 with N-RING1B was 1.9 ± 0.3 μM, accompanied by a large enthalpic contribution of −26.6 kcal/mol, indicating that there is a net unfavorable entropic contribution of 18.8 kcal/mol. The stoichiometry of the complex was close to 1:1 (in dimer units of PADI4) (Table 1), in agreement with the result of the Job's plots obtained from fluorescence experiments (Fig. S5A). The same experiment performed in the presence of GSK484 indicated that the interaction of PADI4 with N-RING1B was completely abolished (Fig. 4C, Table 1).

To sum up, we concluded that N-RING1B could bind to PADI4 with a low-micromolar affinity.

3.3.2. *Affinity of the C-terminal region (C-RING1B) to PADI4*

We used steady-state fluorescence and the rest of the spectroscopic and biophysical techniques already used for determining the binding between N-RING1B and PADI4 with the same aim, to detect the binding between PADI4 and C-RING1B.

A variation in fluorescence intensity by excitation at 280 nm was observed when the complex of PADI4/C-RING1B was formed (Fig. 5A), but there were no changes in the maximum wavelength of the spectrum. Similar variations were observed by excitation at 295 nm. These findings indicate that the environment around some of the aromatic residues of at least one of the proteins was changed upon complex formation, as it was already found for N-RING1B.

Next, we carried out far-UV CD measurements, with the aim of further supporting the results obtained by fluorescence. The far-UV addition spectrum was similar to that of the complex (Fig. 5B). The fact that far-UV CD spectra were similar (in contrast to what happened with the PADI4/N-RING1B complex, Fig. 3B) could mean that both polypeptide chains were bound without any changes in their secondary structures. On the light of this observation, the findings previously obtained for N-RING1B could also be due to a partial folding-upon-binding of some disordered regions of that isolated fragment, which are more abundant compared to those present in C-RING1B, as the latter fragment includes the large well-folded ubiquitin-like domain. Under such hypothesis, the variations observed in the far-UV CD spectrum of the PADI4/N-RING1B complex (Fig. 3B) would mainly be associated with the binding of the N-terminal region of RING1B to the enzyme.

We also carried out thermal denaturations followed by far-UV CD. We observed that the thermal denaturation midpoint of C-RING1B was similar (53.7 ± 0.1 °C or 327.7 ± 0.1 K) to that measured in the complex (53.2 ± 0.3 °C or 326.2 ± 0.2 K) (Fig. 5C). As it happened with the steady-state far-UV CD spectra, these results also differed from those found for N-RING1B (Fig. 3C).

Finally, we acquired 2D ^{1}H-^{15}N HSQC NMR spectra of C-RING1B in the presence and absence of PADI4 (Fig. 6). The presence of the enzyme caused changes in the chemical shifts of many cross-peaks (blue and black cross-peaks in Fig. 6); in some cases, as it happened for the cross-peak of indole side-chain of the sole tryptophan residue of C-RING1B (Trp319, with the proton of the aromatic moiety around 9.70 ppm), it

Table 1
Thermodynamic parameters, as determined by ITC, for the binding of PADI4 to the fragments of RING1B.[a]

Fragment		K_a (M^{-1})	K_d (μM)	ΔG (kcal/mol)	ΔH (kcal/mol)	−TΔS (kcal/mol)	n
N-RING1B	- GSK484	$5.4 \cdot 10^5$	1.9	−7.8	−26.6	18.8	1.0
	+ GSK484	–	–	–	–	–	–
C-RING1B	- GSK484	$4.0 \cdot 10^5$	2.5	−7.6	−14.6	7.0	1.1
	+ GSK484	–	–	–	–	–	–

[a] Relative error in K_a and K_d is 20 %, absolute error in ΔH and −TΔS is 0.4 kcal/mol, and absolute error in ΔG is 0.1 kcal/mol. Experiments in the presence of GSK484 did not yield any result.

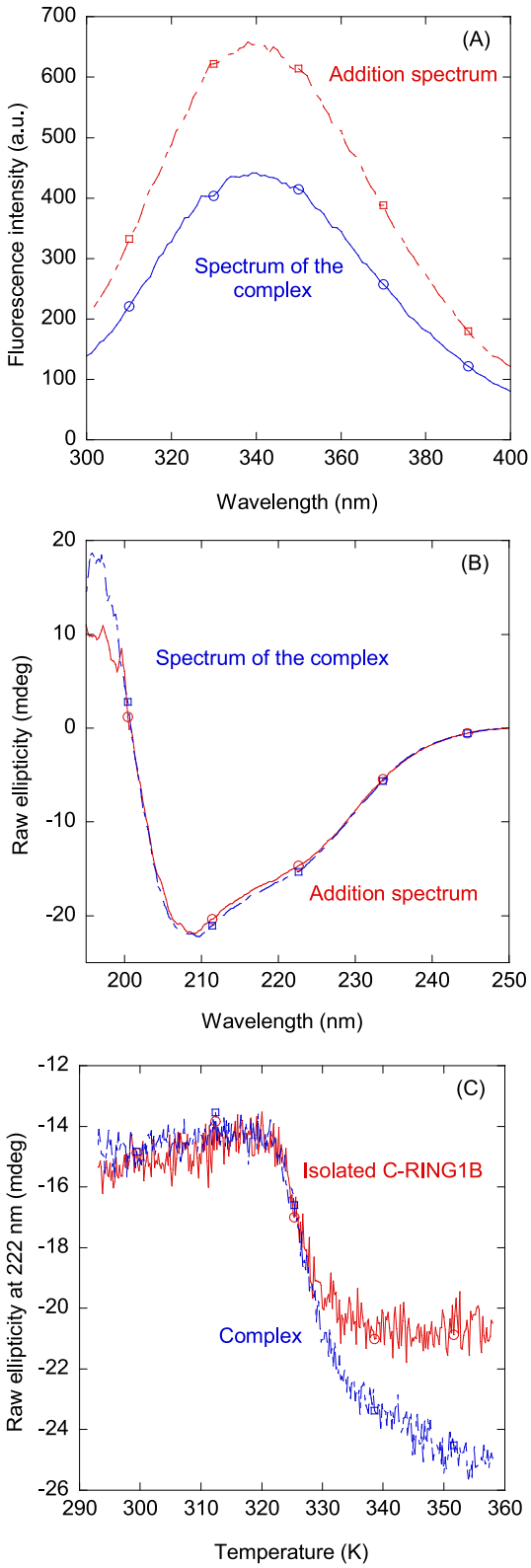

Fig. 5. Binding of C-RING1B to PADI4 as monitored by spectroscopic techniques: (A) Fluorescence spectrum obtained by excitation at 280 nm of the PADI4/C-RING1B complex, and addition spectrum obtained by the sum of the spectra of the two isolated macromolecules. (B) Far-UV CD spectrum of the PADI4/C-RING1B complex, and addition spectrum obtained by the sum of the spectra of the two isolated macromolecules. All experiments were performed at 25 °C. (C) Thermal denaturation scans of isolated C-RING1B and the complex PADI4/C-RING1B followed by far-UV CD.

disappeared in the presence of PADI4. This result confirms the fluorescence findings, since it indicates that Trp319 was directly involved in binding (Fig. 6). However, when the same amount of GSK484 as that of PADI4 was added to the solution, the chemical shifts of the cross-peaks that were displaced upon PADI4 addition moved towards their native-like positions in isolated C-RING1B (red cross-peaks in Fig. 6; see, for instance, the cross-peak around 8.0 (^{1}H) and 129 (^{15}N) ppm). These variations indicate that C-RING1B binds either directly to the active site of PADI4 or to another region that is allosterically modulated by the presence of GSK484 bound in the active site of the enzyme.

Finally, we carried out fluorescence titrations to quantitatively measure the affinity of the two polypeptides, by keeping constant the concentration of PADI4 and increasing the concentration of C-RING1B. The results (Fig. 7A) indicate that the dissociation constant, K_d, was 10 ± 3 μM. This value was identical to that measured for the N-RING1B. Therefore, both isolated fragments had the same affinity for the enzyme. We also made the Job's plots for this titration [75–77], which yields an intersection point of the two lines at 2.0 (Fig. S5 B), corresponding to the rate of [C-RING1B]/[PADI4$_{protomer}$].

Again, in this case, we also used ITC to determine the thermodynamic binding parameters, *i.e.*, the enthalpy and the entropy of the binding reaction (Fig. 7B). According to the calorimetric experiments, the dissociation constant for the interaction of PADI4 with C-RING1B was 2.5 ± 0.5 μM, accompanied by a large apparent enthalpic contribution of −14.6 kcal/mol, indicating that there is a net unfavorable entropic contribution unfavorable. The stoichiometry of the complex was 1:1 (in dimer units of PADI4) (Table 1), in agreement with the result of the Job's plots from fluorescence (Fig. S5B). The same experiment performed in the presence of GSK484 indicated that the interaction of PADI4 with N-RING1B was completely abolished (Fig. 7C, Table 1).

To sum up, we concluded that there was evidence that C-RING1B could bind to PADI4 with a low-micromolar affinity.

3.4. Structural prediction of the complex PADI4/RING1B complex

Protein-protein docking was used to predict some of the key features of the complex between PADI4 and RING1B. To improve the reliability of the calculations, due to the structural complexity and large flexibility of RING1B, this protein was divided into two main fragments, and the largely disordered region between them (residues 135–227) was neglected. Thus, in the simulations the fragment N-RING1B (residues 1–134) was shorter compared to the construct used in our other experiments, whereas the fragment C-RING1B (residues 228–336) was identical. In contrast, PADI4 was considered in its entirety, in the homodimeric form.

The results indicated quite different conformational preferences for the association of the two fragments N-RING1B and C-RING1B on the surface of PADI4, as shown in Fig. 8. In fact, C-RING1B showed a distinct affinity to bind in correspondence with the active site of PADI4 (Fig. 8A) in the prediction obtained with the algorithm ClusPro [66]. This algorithm was selected over other popular ones [67] because it led to a molecular complex with a considerably more favorable binding energy (see Table S1), calculated according to the MM/GBSA methodology [69]. Furthermore, similarly to most other algorithms explored, but at variance with some of them, it also predicted the correct stoichiometry of the complex, consisting of two monomers of C-RING1B bound to each PADI4 homodimer. In fact, due to the symmetry of the structure of the PADI4 homodimer, a docking pose that overlaps with its symmetrical image makes the existence of the two poses mutually exclusive, when they are considered together. These results agree with what was found in the ITC measurements (Table 1) and in the Job's plots obtained from fluorescence experiments (Fig. S5).

Notably, ClusPro was one of the few algorithms that also predicted that the binding interface of C-RING1B could directly involve the key residue Trp319 (Fig. 8A). This result agrees at best with our experimental findings, which include both NMR data (Fig. 6) and fluorescence.

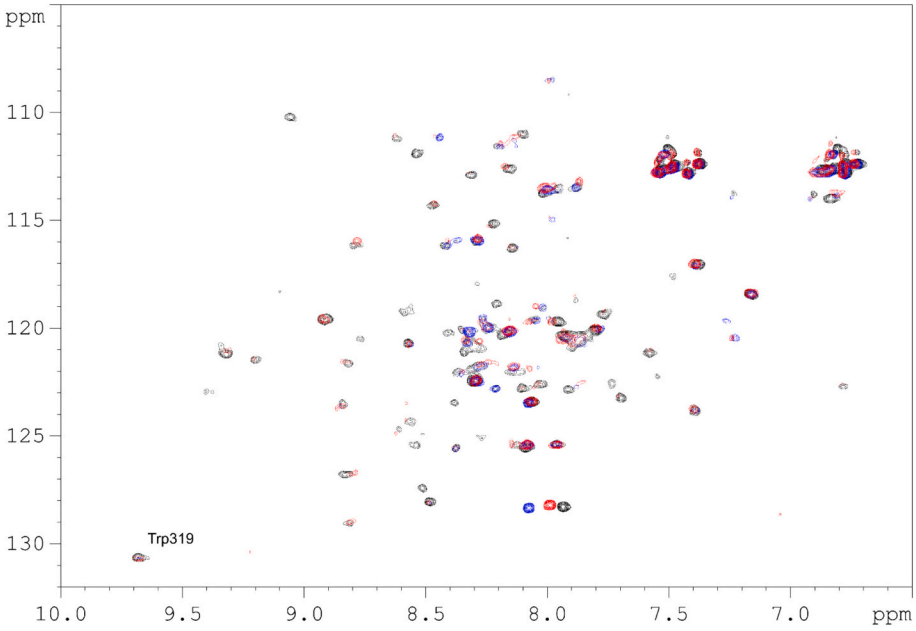

Fig. 6. NMR experiments of the association of PADI4 and C-RING1B: 2D ^{1}H-^{15}N HSQC NMR spectra of C-RING1B in the absence (black lines) or in the presence of PADI4 (blue lines), and when PADI4 was present together with the enzymatic GSK484 inhibitor of PADI4 (red lines). The indole proton of the aromatic side-chain of Trp319, being the sole tryptophan in the fragment, is indicated. All experiments were carried out at 25 °C. (For interpretation of the references to colour in this figure legend, the reader is referred to the web version of this article.)

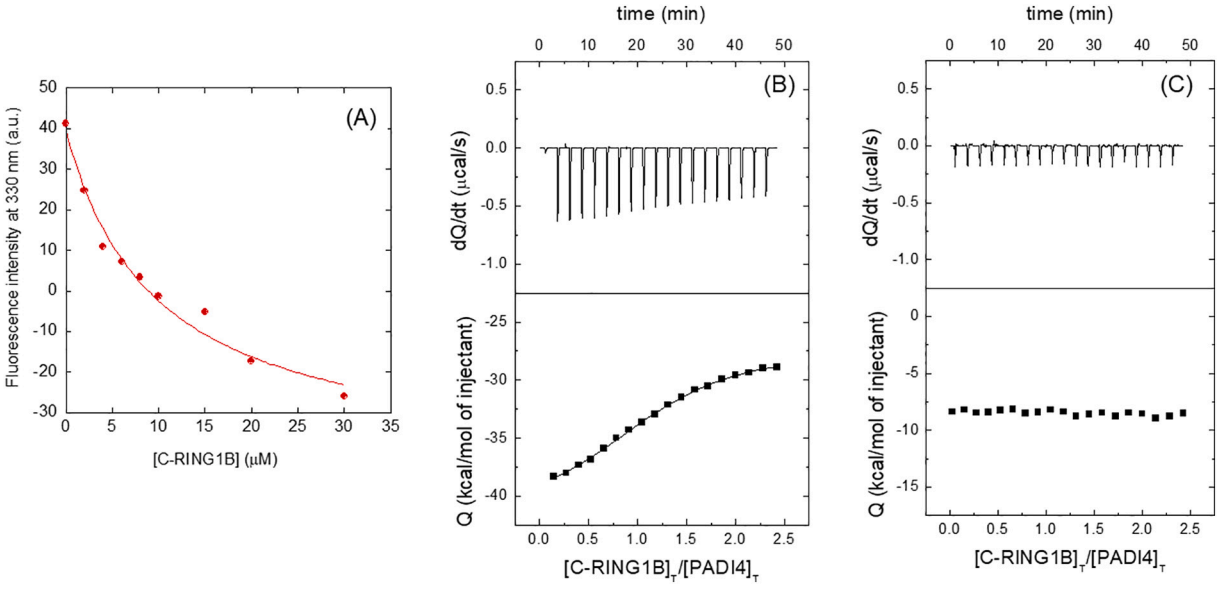

Fig. 7. Quantitative determination of the binding of C-RING1B to PADI4 as monitored by biophysical techniques: (A) Titration curve monitoring the changes in the fluorescence at 330 nm when C-RING1B was added to PADI4. The fluorescence intensity is the relative signal after removal of the corresponding blank. The line through the data is the fitting to Eq. (1). Calorimetric titrations for C-RING1B binding to PADI4 in the absence (B) and presence of GSK484 (C). Upper panels show the thermograms (thermal power as a function of time) and lower panels show the binding isotherms (ligand-normalized heat effects *per* injection as a function of the molar ratio in the calorimetric cell). Continuous lines correspond to the fitting curves according to an interaction model with a single ligand binding site. All experiments were carried out at 25 °C.

Perhaps more importantly, in simulation the residue Trp319 was almost directly in contact (distance <5 Å) with the catalytic Cys645 of PADI4 (Fig. 8A). In close spatial proximity to Trp319 (distance <7 Å), the nearest arginine residue is Arg231, which could end up being driven towards the catalytic site of PADI4 and, therefore, might be citrullinated in the presence of Ca(II) ions.

It should also be noted that ZDock [78], which was the sole other algorithm beside ClusPro to indicate the binding of C-RING1B in the active site of PADI4 as the most favorable docking pose (although with a markedly lower binding energy; see again Table S1), predicted a geometry qualitatively similar for the binding complex, with both Trp319 and Arg231 in proximity of the catalytic site of PADI4.

In sharp contrast with C-RING1B, the fragment N-RING1B was not predicted to bind in correspondence with the active site of PADI4. ClusPro was again the predictor that provided by far the most favorable binding energy (Table S2), similar to fragment C-RING1B. As shown in

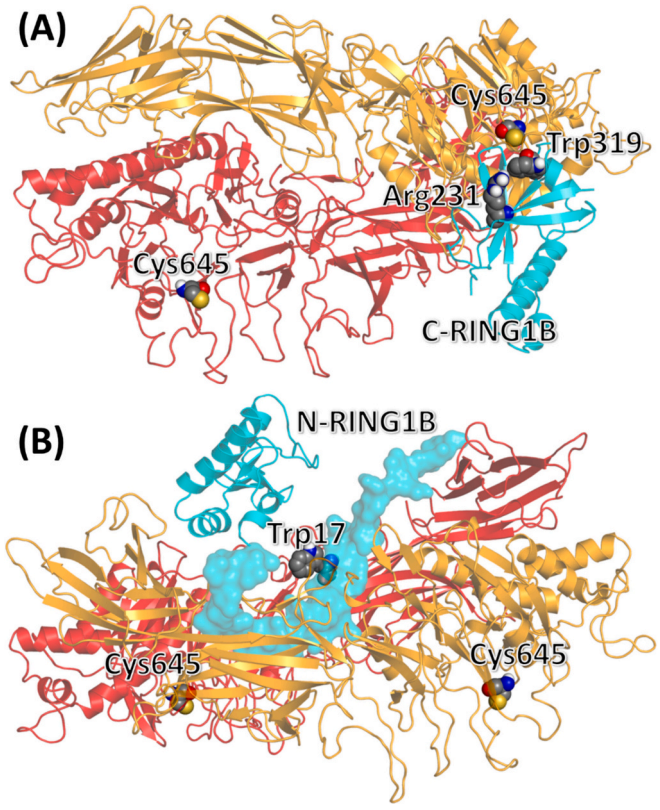

Fig. 8. Modeling of the binding complex of PADI4 and the two fragments C-RING1B and N-RING1B in the prediction of the algorithm ClusPro. The two dimers of PADI4 (yellow and red), as well as either fragment of RING1B (cyan), are represented as ribbons. The catalytic residues Cys645 of PADI4 are explicitly shown (van der Waals representation) and labeled. (A) Prediction for C-RING1B (residues 228–336); the key residues Trp319 and Arg231 are labeled. (B) Prediction for N-RING1B (residues 1–134); its less compact region (residues 1–40) is evidenced (cyan surface), and residue Trp17 is labeled. (For interpretation of the references to colour in this figure legend, the reader is referred to the web version of this article.)

Fig. 8B, the binding of N-RING1B appeared to be driven by the less compact region of the portion (residues 1–134) considered in simulation for this fragment, and in particular, by the first ~40 residues. The target region of N-RING1B was either side of the crevice at the homodimeric interface of PADI4. Among the residues of N-RING1B involved in the binding, residue Trp17 played a role, as it was solvent-exposed in the unbound protein fragment and became partially buried in the PADI4 crevice upon the binding. Again, in this case, as it happens with Trp319 at C-RING1B, this may contribute to explain the fluorescence results obtained in our *in vitro* experiments.

4. Discussion and conclusion

Over the years, there has been little improvement in the survival rate of patients with hard-to-treat cancers such as GBM, PDAC, and COAD. These cancer types grow aggressively, are detected at late-stage diagnosis, and are extremely resistant to therapy [79–81]. More specific and effective treatments are urgently needed for these cancers given their poor prognoses. To guarantee more successful treatments, we need to enhance the early detection of these aggressive tumors, boost the effectiveness of existing cancer drugs, develop new ones, or find new targets [82]. Considering the significance of PADI4 and RING1B in cancer, we explored the possibility and consequences of a mutual direct interaction of these two proteins in this context. In fact, it is intriguing to consider the potential effects of this newly discovered interaction on the development and progression of cancer, and in the development of new cancer therapies based on RING1B citrullination.

The discovery of the binding between RING1B and PADI4 was prompted by an initial hypothesis. We had recently shown that PADI4 binds to RYBP [53], which in turn binds also to RING1B, forming the non-canonical PRC1 complexes. They are also both capable of binding to the oncoprotein NUPR1 and its paralogue NUPR1 IDP [32,33], and they are also implicated in tumor pathways that involve a number of other proteins in common [53], To test the hypothesis of a well-defined complex between the two proteins, we carried out several *in cellulo*, *in vitro*, and *in silico* experiments. We hypothesized that such interaction could also be detected in the most direct and indisputable way in cancer cells, and we tested it with GBM, PDAC, and COAD cell lines. In fact, in all tumor lines we tested, we observed that RING1B and PADI4 interacted in the nucleus and cytosol. Furthermore, the enzymatic PADI4 inhibitor GSK484 hampered the interaction of the two proteins, similarly to its effect in PADI4/RYBP binding [53]. These results suggested that RING1B was bound to the active site of the enzyme or to another site in PADI4 allosterically coupled with the active site. Our *in cellulo* assays also showed that the effect of GSK484 varied among the different tumor cell lines with higher effect on the nucleus where PADI4 and RING1B were mostly co-expressed.

The measured K_d of the complex of PADI4 with the two separate fragments of RING1B, N-RING1B and C-RING1B, was similar (~10 μM according to steady-state fluorescence, and ~2 μM according to ITC). These values are comparable to that of the complexes of PADI4 with RYBP (~10 μM) [53], with the model IDP and multifunctional oncoprotein NUPR1 (~15 μM) [52], with the well-folded armadillo domain of plakophilin 1 (~8 μM) [50], and with importin α3 (~5 μM) [49]. Thus, it appears increasingly clear that PADI4 shows a similar low affinity with all their molecular partners in the different protein cross-talks in which is involved. It is interesting to note that the N-terminal region of RING1B is mostly disordered [34], but in the presence of PADI4 a folding-upon-binding event possibly occurs. This behavior was similar to that found for the other two IDPs that were already found to be partners of PADI4: RYBP and NUPR1 [52,53].

More information on the association of PADI4 and RING1B was also provided by the ITC measurements *in vitro*. The interaction of PADI4 with both RING1B fragments was strongly exothermic (−26.6 and −14.6 kcal/mol for N-RING1B and C-RING1B, respectively), indicating a large unfavorable interaction entropy (18.8 and 7.0 kcal/mol for N-RING1B and C-RING1B, respectively), and further suggesting that the binding might proceed with a sort of structural rearrangement that entropically overwhelms the expected favorable desolvation entropy. When performing titrations in the presence of GSK484, no interaction between PADI4 and either C-RING1B or N-RING1B was observed. This finding may reflect either a competitive inhibition (RING1B fragments bind to the active site, as GSK484 does) or an allosteric inhibition (RING1B fragments bind to another PADI4 site, which is allosterically regulated by the binding of GSK484). In either case, the modulation of the interaction of PADI4 with both RING1B fragments exerted by GSK484 represents additional evidence for their direct interaction.

Our molecular docking simulations indicated different locations for the binding of the two fragments N-RING1B and C-RING1B, with only the latter targeting the active site of PADI4. In the context of the intact protein RING1B, these two binding locations are not mutually exclusive, and it is possible that both fragments could participate in the formation of the overall molecular complex. An additional role, although likely of minor importance, could be played by a largely disordered region of RING1B (residues 135–227) neglected in our calculations. The simulations further suggest that two tryptophans (Trp17 and Trp319) contribute to the binding of either fragment, in agreement with the NMR and fluorescence results. In particular, Trp319 in C-RING1B directly targets the active sites of PADI4. This observation, which contributes to explain our competitive inhibition experiments, is of special relevance because it suggests that Arg231 could get citrullinated under opportune biological conditions.

PADI4 is the enzyme responsible for the catalytic conversion of arginine residues to citrulline [39]. RING1B, on the other hand, is a component of the ubiquitin ligase complex. The interaction between PADI4 and RING1B could potentially affect several pathways implicated in cancer progression. For instance, it is well known that the transcription factor glycogen synthase kinase 3 beta (GSK3β) maintains the epithelial phenotype through the citrullination of arginine residue at the N-terminal end, regulated by PADI4. This process inhibits the transforming growth factor β (TGFβ) pathway, and therefore the epithelial-to-mesenchymal transition (EMT). As an example, in breast cancer, the knockdown of PADI4 in MCF-7 cells results to a decrease of the expression of GSK3β, the stabilization of Smad4, and the activation of the TGFβ signaling pathway, reducing E-cadherin and promoting vimentin expression, leading to the stimulation of tumor migration and invasion [71]. On the other hand, RING1B binds to the latent transforming growth factor beta binding protein 2 (LTBP2) promoter, which can negatively regulate the expression of TGFβ, and therefore its gene silence can activate the TGFβ signaling pathway, which promotes the invasion and metastasis in melanoma. This process depends on the ubiquitination activity of RNF2 [83]. We hypothesize that the interaction between PADI4 and RING1B, and the possible citrullination of the latter, could lead to an altered activity of the RING1B ubiquitination capacity, therefore promoting cancer progression in different types of cancer through the activation of the TGFβ signaling pathway.

The interaction of PADI4/RING1B in the nucleus might also have implications for epigenetic regulation. In fact, PADI4 is involved in citrullination, a PTM that can alter chromatin structure and gene expression patterns [84], and RING1B belongs to the family of PcG proteins, which are epigenetic gene silencers with the ability to affect a wide range of biological functions [20]. The interaction between these two proteins might affect epigenetic regulation by modulating histone modifications and chromatin remodeling, leading to aberrant gene expression profiles associated with cancer initiation and progression. Along this line, in breast cancer cell lines, the silencing of RING1B caused a decrease in histone H2A ubiquitination level, and therefore, it induced TGFβ-induced phenotypic changes required for migration and invasion as observed both *in vitro* and *in vivo* [85].

To conclude, our demonstration of a direct interaction between PADI4 and RING1B opens several interesting hypotheses on the biological relevance of their molecular cross-talk in cells. In addition, given the direct participation of both proteins in well-known tumor pathways, their binding opens new possibilities to impact on such pathological processes, possibly indicating novel opportunities in cancer therapies. Although we caution for the need of further accurate studies on this topic, we also envision new scenarios that can be explored by building upon our findings along a number of directions, such as in the field of cancer epigenetics.

CRediT authorship contribution statement

Salome Araujo-Abad: Writing – review & editing, Writing – original draft, Methodology, Investigation, Formal analysis. **Bruno Rizzuti:** Writing – review & editing, Writing – original draft, Methodology, Investigation, Formal analysis, Conceptualization. **Lourdes Soto-Conde:** Investigation, Formal analysis. **Miguel Vidal:** Writing – review & editing, Resources. **Olga Abian:** Writing – review & editing, Writing – original draft, Project administration, Investigation, Funding acquisition, Formal analysis. **Adrian Velazquez-Campoy:** Writing – review & editing, Writing – original draft, Project administration, Methodology, Investigation, Funding acquisition, Formal analysis, Conceptualization. **José L. Neira:** Writing – review & editing, Writing – original draft, Methodology, Investigation, Funding acquisition, Formal analysis, Conceptualization. **Camino de Juan Romero:** Writing – review & editing, Writing – original draft, Project administration, Methodology, Investigation, Funding acquisition, Formal analysis, Conceptualization.

Declaration of competing interest

The authors declare that they have no known competing financial interests or personal relationships that could have appeared to influence the work reported in this paper.

Data availability

Data will be made available on request.

Acknowledgements

This research was funded by Spanish Ministry of Economy and Competitiveness and European ERDF Funds (MCIU/AEI/FEDER, EU) [PID2021-127296OB-I00 to AVC, CP19/00095 to CdJ]; Fondo de Investigaciones Sanitarias from Instituto de Salud Carlos III, and European Union (ERDF/ESF, "Investing in your future") [PI21/00394 to OA and PI22/00824 to CdJ]; Diputación General de Aragón ["Protein targets and Bioactive Compounds group" E45-23R to AVC, and "Digestive Pathology Group" B25-23R to OA]; and Comunidad Valenciana [CIAICO 2021/0135 to CdJ and JLN]. The funders had no role in the study design, data collection and analysis, decision to publish, or preparation of the manuscript.

We thank the two anonymous reviewers for helpful suggestions and discussions. We thank Prof. Shinya Toyokuni for handling the manuscript.

Appendix A. Supplementary data

Supplementary data to this article can be found online at https://doi.org/10.1016/j.ijbiomac.2024.133163.

References

[1] J.A. Simon, R.E. Kingston, Occupying chromatin: Polycomb mechanisms for getting to genomic targets, stopping transcriptional traffic, and staying put, Mol. Cell 49 (2013) 808–824, https://doi.org/10.1016/J.MOLCEL.2013.02.013.
[2] J.A. Simon, R.E. Kingston, Mechanisms of Polycomb gene silencing: knowns and unknowns, Nat. Rev. Mol. Cell Biol. 10 (2009) 697–708, https://doi.org/10.1038/NRM2763.
[3] B. Schuettengruber, G. Cavalli, Recruitment of Polycomb group complexes and their role in the dynamic regulation of cell fate choice, Development 136 (2009) 3531–3542, https://doi.org/10.1242/DEV.033902.
[4] L. Morey, K. Helin, Polycomb group protein-mediated repression of transcription, Trends Biochem. Sci. 35 (2010) 323–332, https://doi.org/10.1016/J.TIBS.2010.02.009.
[5] R. Margueron, D. Reinberg, The Polycomb complex PRC2 and its mark in life, Nature 469 (7330) (2011) 343–349, https://doi.org/10.1038/nature09784.
[6] H.L. Chan, L. Morey, Emerging roles for Polycomb-group proteins in stem cells and cancer, Trends Biochem. Sci. 44 (2019) 688–700, https://doi.org/10.1016/J.TIBS.2019.04.005.
[7] W.A. Flavahan, E. Gaskell, B.E. Bernstein, Epigenetic plasticity and the hallmarks of cancer, Science 357 (2017), https://doi.org/10.1126/SCIENCE.AAL2380.
[8] B. Schuettengruber, H.M. Bourbon, L. Di Croce, G. Cavalli, Genome regulation by Polycomb and Trithorax: 70 years and counting, Cell 171 (2017) 34–57, https://doi.org/10.1016/J.CELL.2017.08.002.
[9] S. Gao, S.Y. Wang, X. Da Zhang, H. Wu, D. Pang, Low expression of the Polycomb protein RING1 predicts poor prognosis in human breast cancer, Front. Oncol. 10 (2021) 1, https://doi.org/10.3389/FONC.2020.618768/FULL.
[10] A.P. Bracken, N. Dietrich, D. Pasini, K.H. Hansen, K. Helin, Genome-wide mapping of Polycomb target genes unravels their roles in cell fate transitions, Genes Dev. 20 (2006) 1123–1136, https://doi.org/10.1101/GAD.381706.
[11] L. Kaustov, H. Ouyang, M. Amaya, A. Lemak, N. Nady, S. Duan, G.A. Wasney, Z. Li, M. Vedadi, M. Schapira, J. Min, C.H. Arrowsmith, Recognition and specificity determinants of the human cbx chromodomains, J. Biol. Chem. 286 (2011) 521–529, https://doi.org/10.1074/JBC.M110.191411.
[12] Z. Gao, J. Zhang, R. Bonasio, F. Strino, A. Sawai, F. Parisi, Y. Kluger, D. Reinberg, PCGF homologs, CBX proteins, and RYBP define functionally distinct PRC1 family complexes, Mol. Cell 45 (2012) 344–356, https://doi.org/10.1016/J.MOLCEL.2012.01.002.
[13] D.J. Grau, J.M. Antao, R.E. Kingston, Functional dissection of Polycomb repressive complex 1 reveals the importance of a charged domain, Cold Spring Harb. Symp. Quant. Biol. 75 (2010) 61–70, https://doi.org/10.1101/SQB.2010.75.056.
[14] H. Richly, L. Aloia, L. Di Croce, Roles of the Polycomb group proteins in stem cells and cancer, Cell Death Dis. 9 (2) (2011) e204, https://doi.org/10.1038/cddis.2011.84.

[15] Y. Yamamoto, A. Abe, N. Emi, Clarifying the impact of polycomb complex component disruption in human cancers, Mol. Cancer Res. 12 (2014) 479–484, https://doi.org/10.1158/1541-7786.MCR-13-0596/79714/AM/CLARIFYING-THE-IMPACT-OF-POLYCOMB-COMPLEX.
[16] Y. Xiong, B. Hu, L. Wei, D. Jiang, M. Zhu, Upregulated expression of polycomb protein Ring1 contributes to poor prognosis and accelerated proliferation in human hepatocellular carcinoma, Tumour Biol. 36 (2015) 9579–9588, https://doi.org/10.1007/S13277-015-3721-7/FIGURES/6.
[17] Y. Zhou, C. Wan, Y. Liu, L. Lv, B. Chen, R. Ni, Y. Huang, Y. Li, X. Zheng, D. Yang, G. Mao, Q. Xue, Polycomb group oncogene RING1 is over-expressed in non-small cell lung cancer, Pathol. Oncol. Res. 20 (2014) 549–556, https://doi.org/10.1007/S12253-013-9727-9/FIGURES/5.
[18] A. Grzenda, T. Ordog, R. Urrutia, Polycomb and the emerging epigenetics of pancreatic cancer, J. Gastrointest. Cancer 42 (2011) 100–111, https://doi.org/10.1007/S12029-011-9262-4/FIGURES/1.
[19] J. Shen, P. Li, X. Shao, Y. Yang, X. Liu, M. Feng, Q. Yu, R. Hu, Z. Wang, The E3 ligase ring1 targets p53 for degradation and promotes cancer cell proliferation and survival, Cancer Res. 78 (2018) 359–371, https://doi.org/10.1158/0008-5472.CAN-17-1805/653129/AM/THE-E3-LIGASE-RING1-TARGETS-P53-FOR-DEGRADATION.
[20] Q. Yan, B. jie Chen, S. Hu, S. li Qi, L. yun Li, J. fa Yang, H. Zhou, C. chen Yang, L. jian Chen, J. Du, Emerging role of RNF2 in cancer: from bench to bedside, J. Cell. Physiol. 236 (2021) 5453–5465, https://doi.org/10.1002/JCP.30260.
[21] R.J. Deshaies, C.A.P. Joazeiro, RING domain E3 ubiquitin ligases, Annu. Rev. Biochem. 78 (2009) 399–434, https://doi.org/10.1146/ANNUREV.BIOCHEM.78.101807.093809.
[22] K.L.B. Borden, RING domains: master builders of molecular scaffolds? J. Mol. Biol. 295 (2000) 1103–1112, https://doi.org/10.1006/JMBI.1999.3429.
[23] Z. Li, R. Cao, M. Wang, M.P. Myers, Y. Zhang, R.M. Xu, Structure of a Bmi-1-Ring1B polycomb group ubiquitin ligase complex, J. Biol. Chem. 281 (2006) 20643–20649, https://doi.org/10.1074/JBC.M602461200.
[24] P.S. Brzovic, P. Rajagopal, D.W. Hoyt, M.C. King, R.E. Klevit, Structure of a BRCA1-BARD1 heterodimeric RING-RING complex, Nat. Struct. Biol. 8 (2001) 833–837, https://doi.org/10.1038/NSB1001-833.
[25] A. Czypionka, O.R. De Los Paños, M.G. Mateu, F.N. Barrera, E. Hurtado-Gómez, J. Gómez, M. Vidal, J.L. Neira, The isolated C-terminal domain of Ring1B is a dimer made of stable, well-structured monomers, Biochemistry 46 (2007) 12764–12776, https://doi.org/10.1021/BI701343Q.
[26] I. Bezsonova, J.R. Walker, J.P. Bacik, S. Duan, S. Dhe-Paganon, C.H. Arrowsmith, Ring1B contains a ubiquitin-like docking module for interaction with Cbx proteins, Biochemistry 48 (2009) 10542–10548, https://doi.org/10.1021/BI901131U/SUPPL_FILE/BI901131U_SI_002.PDF.
[27] J.L. Neira, M. Román-Trufero, L.M. Contreras, J. Prieto, G. Singh, F.N. Barrera, M. L. Renart, M. Vidal, The transcriptional repressor RYBP is a natively unfolded protein which folds upon binding to DNA, Biochemistry 48 (2009) 1348–1360, https://doi.org/10.1021/BI801933C.
[28] E. Garcia, C. Marcos-Gutiérrez, M. Del Mar Lorente, J.C. Moreno, M. Vidal, RYBP, a new repressor protein that interacts with components of the mammalian Polycomb complex, and with the transcription factor YY1, EMBO J. 18 (1999) 3404–3418, https://doi.org/10.1093/EMBOJ/18.12.3404.
[29] C.J. Simoes da Silva, R. Simón, A. Busturia, Epigenetic and non-epigenetic functions of the RYBP protein in development and disease, Mech. Ageing Dev. 174 (2018) 111–120, https://doi.org/10.1016/J.MAD.2018.03.011.
[30] I. Bajusz, S. Henry, E. Sutus, G. Kovács, M.K. Pirity, Evolving role of RING1 and YY1 binding protein in the regulation of germ-cell-specific transcription, Genes (Basel) 10 (2019), https://doi.org/10.3390/GENES10110941.
[31] M. de Napoles, J.E. Mermoud, R. Wakao, Y.A. Tang, M. Endoh, R. Appanah, T. B. Nesterova, J. Silva, A.P. Otte, M. Vidal, H. Koseki, N. Brockdorff, Polycomb group proteins Ring1A/B link ubiquitylation of histone H2A to heritable gene silencing and X inactivation, Dev. Cell 7 (2004) 663–676, https://doi.org/10.1016/J.DEVCEL.2004.10.005.
[32] P. Santofimia-Castaño, B. Rizzuti, Á.L. Pey, P. Soubeyran, M. Vidal, R. Urrutia, J. L. Iovanna, J.L. Neira, Intrinsically disordered chromatin protein NUPR1 binds to the C-terminal region of polycomb RING1B, Proc. Natl. Acad. Sci. U. S. A. 114 (2017), https://doi.org/10.1073/pnas.1619932114.
[33] J.L. Neira, M.B. López, P. Sevilla, B. Rizzuti, A. Cámara-Artigas, M. Vidal, J. L. Iovanna, The chromatin nuclear protein NUPR1L is intrinsically disordered and binds to the same proteins as its paralogue, Biochem. J. 475 (2018), https://doi.org/10.1042/BCJ20180365.
[34] A.I. Martínez-Gómez, S. Villegas, D. Aguado-Llera, J. Bacarizo, A. Cámara-Artigas, M. Vidal, J.L. Neira, The isolated N terminus of Ring1B is a well-folded, monomeric fragment with native-like structure, Protein Eng. Des. Sel. 27 (2014) 1–11, https://doi.org/10.1093/PROTEIN/GZT056.
[35] M.L. Bentley, J.E. Corn, K.C. Dong, Q. Phung, T.K. Cheung, A.G. Cochran, Recognition of UbcH5c and the nucleosome by the Bmi1/Ring1b ubiquitin ligase complex, EMBO J. 30 (2011) 3285–3297, https://doi.org/10.1038/EMBOJ.2011.243.
[36] A.E. Yuzhalin, Citrullination in Cancer, Cancer Res. 79 (2019) 1274–1284, https://doi.org/10.1158/0008-5472.CAN-18-2797.
[37] N.S. Gudmann, N.U.B. Hansen, A.C.B. Jensen, M.A. Karsdal, A.S. Siebuhr, Biological relevance of citrullinations: diagnostic, prognostic and therapeutic options, Autoimmunity 48 (2015) 73–79, https://doi.org/10.3109/08916934.2014.962024.
[38] A. Ishigami, N. Maruyama, Importance of research on peptidylarginine deiminase and citrullinated proteins in age-related disease, Geriatr Gerontol Int 10 Suppl 1 (2010), https://doi.org/10.1111/J.1447-0594.2010.00593.X.
[39] B. György, E. Tóth, E. Tarcsa, A. Falus, E.I. Buzás, Citrullination: a posttranslational modification in health and disease, Int. J. Biochem. Cell Biol. 38 (2006) 1662–1677, https://doi.org/10.1016/J.BIOCEL.2006.03.008.
[40] S. Ying, S. Dong, A. Kawada, T. Kojima, S. Chavanas, M.C. Méchin, V. Adoue, G. Serre, M. Simon, H. Takahara, Transcriptional regulation of peptidylarginine deiminase expression in human keratinocytes, J. Dermatol. Sci. 53 (2009) 2–9, https://doi.org/10.1016/J.JDERMSCI.2008.09.009.
[41] D.J. Slade, S. Horibata, S.A. Coonrod, P.R. Thompson, A novel role for protein arginine deiminase 4 in pluripotency: the emerging role of citrullinated histone H1 in cellular programming, Bioessays 36 (2014) 736–740, https://doi.org/10.1002/BIES.201400057.
[42] E. Witalison, P. Thompson, L. Hofseth, Protein arginine deiminases and associated citrullination: physiological functions and diseases associated with dysregulation, Curr. Drug Targets 16 (2015) 700–710, https://doi.org/10.2174/1389450116666150202160954.
[43] Y. Wang, R. Chen, Y. Gan, S. Ying, The roles of PAD2- and PAD4-mediated protein citrullination catalysis in cancers, Int. J. Cancer 148 (2021) 267–276, https://doi.org/10.1002/IJC.33205.
[44] C. Yang, Z.Z. Dong, J. Zhang, D. Teng, X. Luo, D. Li, Y. Zhou, Peptidylarginine deiminases 4 as a promising target in drug discovery, Eur. J. Med. Chem. 226 (2021) 113840, https://doi.org/10.1016/J.EJMECH.2021.113840.
[45] H.C. Hung, C.Y. Lin, Y.F. Liao, P.C. Hsu, G.J. Tsay, G.Y. Liu, The functional haplotype of peptidylarginine deiminase IV (S55G, A82V and A112G) associated with susceptibility to rheumatoid arthritis dominates apoptosis of acute T leukemia Jurkat cells, Apoptosis 12 (2007) 475–487, https://doi.org/10.1007/S10495-006-0005-0.
[46] P. Li, H. Yao, Z. Zhang, M. Li, Y. Luo, P.R. Thompson, D.S. Gilmour, Y. Wang, Regulation of p53 target gene expression by peptidylarginine deiminase 4, Mol. Cell. Biol. 28 (2008) 4758, https://doi.org/10.1128/MCB.01747-07.
[47] P. Li, D. Wang, H. Yao, P. Doret, G. Hao, Q. Shen, H. Qiu, X. Zhang, Y. Wang, G. Chen, Y. Wang, Coordination of PAD4 and HDAC2 in the regulation of p53-target gene expression, Oncogene 29 (2010) 3153–3162, https://doi.org/10.1038/onc.2010.51.
[48] J.L. Neira, S. Araujo-Abad, A. Cámara-Artigas, B. Rizzuti, O. Abian, A.M. Giudici, A. Velazquez-Campoy, C. de Juan Romero, Biochemical and biophysical characterization of PADI4 supports its involvement in cancer, Arch. Biochem. Biophys. 717 (2022), https://doi.org/10.1016/J.ABB.2022.109125.
[49] J.L. Neira, B. Rizzuti, O. Abián, S. Araujo-Abad, A. Velázquez-Campoy, C. de Juan Romero, Human enzyme PADI4 binds to the nuclear carrier importin α3, Cells 11 (2022), https://doi.org/10.3390/CELLS11142166.
[50] J.L. Neira, B. Rizzuti, S. Araujo-Abad, O. Abian, M.E. Fárez-Vidal, A. Velazquez-Campoy, C. de Juan Romero, The armadillo-repeat domain of Plakophilin 1 binds to human enzyme PADI4, Biochim. Biophys. Acta, Proteins Proteomics 1871 (2023), https://doi.org/10.1016/J.BBAPAP.2022.140868.
[51] S. Araujo-Abad, B. Rizzuti, A. Villamarin-Ortiz, D. Pantoja-Uceda, C.M. Moreno-Gonzalez, O. Abian, A. Velazquez-Campoy, J.L. Neira, C. de Juan Romero, New insights into cancer: MDM2 binds to the citrullinating enzyme PADI4, Protein Sci. 32 (2023), https://doi.org/10.1002/PRO.4723.
[52] S. Araujo-Abad, J.L. Neira, B. Rizzuti, P. García-Morales, C. de Juan Romero, P. Santofimia-Castaño, J. Iovanna, Intrinsically disordered chromatin protein NUPR1 binds to the enzyme PADI4, J. Mol. Biol. 435 (2023), https://doi.org/10.1016/j.jmb.2023.168033.
[53] S. Araujo-Abad, M. Fuentes-Baile, B. Rizzuti, J.F. Bazán, A. Villamarin-Ortiz, M. Saceda, E. Fernández, M. Vidal, O. Abian, A. Velazquez-Campoy, C. de Juan Romero, J.L. Neira, The intrinsically disordered, epigenetic factor RYBP binds to the citrullinating enzyme PADI4 in cancer cells, Int. J. Biol. Macromol. 246 (2023), https://doi.org/10.1016/J.IJBIOMAC.2023.125632.
[54] S.C. Gill, P.H. von Hippel, Calculation of protein extinction coefficients from amino acid sequence data, Anal. Biochem. 182 (1989) 319–326, https://doi.org/10.1016/0003-2697(89)90602-7.
[55] M.P. Ventero, M. Fuentes-Baile, C. Quereda, E. Perez-Valeciano, C. Alenda, P. Garcia-Morales, D. Esposito, P. Dorado, V.M. Barbera, M. Saceda, Radiotherapy resistance acquisition in glioblastoma. Role of SOCS1 and SOCS3, PLoS One 14 (2019) e0212581, https://doi.org/10.1371/journal.pone.0212581.
[56] M. Fuentes-Baile, D. Bello-Gil, E. Pérez-Valenciano, J.M. Sanz, P. García-Morales, B. Maestro, M.P. Ventero, C. Alenda, V.M. Barberá, M. Saceda, CLyta-DAAO, free and immobilized in magnetic nanoparticles, induces cell death in human cancer cells, Biomolecules 10 (2020) 222, https://doi.org/10.3390/biom10020222.
[57] M. Fuentes-Baile, E. Pérez-Valenciano, P. García-Morales, C. de J. Romero, D. Bello-Gil, V.M. Barberá, Á. Rodríguez-Lescure, J.M. Sanz, C. Alenda, M. Saceda, CLytA-DAAO chimeric enzyme bound to magnetic nanoparticles. A new therapeutical approach for cancer patients? Int. J. Mol. Sci. 22 (2021) 1–24, https://doi.org/10.3390/IJMS22031477.
[58] J.L. Neira, F. Hornos, J. Bacarizo, A. Cámara-Artigás, J. Gómez, The monomeric species of the regulatory domain of tyrosine hydroxylase has a low conformational stability, Biochemistry 55 (2016), https://doi.org/10.1021/acs.biochem.6b00135.
[59] B. Birdsall, R.W. King, M.R. Wheeler, C.A. Lewis, S.R. Goode, R.B. Dunlap, G.C. K. Roberts, Correction for light absorption in fluorescence studies of protein-ligand interactions, Anal. Biochem. 132 (1983) 353–361, https://doi.org/10.1016/0003-2697(83)90020-9.
[60] D. Beckett, Measurement and analysis of equilibrium binding titrations: a beginner's guide, Methods Enzymol. 488 (2011) 1–16, https://doi.org/10.1016/B978-0-12-381268-1.00001-X.
[61] C.A. Royer, S.F. Scarlata, Fluorescence approaches to quantifying biomolecular interactions, Methods Enzymol. 450 (2008) 79–106, https://doi.org/10.1016/S0076-6879(08)03405-8.

[62] J. Cavanagh, W.J. Fairbrother, A.G. Palmer, N.J. Skelton, Protein NMR Spectroscopy: Principles and Practice, 2nd edition, 2007.
[63] G. Bodenhausen, D.J. Ruben, Natural abundance nitrogen-15 NMR by enhanced heteronuclear spectroscopy, Chem. Phys. Lett. 69 (1980) 185–189, https://doi.org/10.1016/0009-2614(80)80041-8.
[64] M. Piotto, V. Saudek, V. Sklenář, Gradient-tailored excitation for single-quantum NMR spectroscopy of aqueous solutions, J. Biomol. NMR 2 (1992) 661–665, https://doi.org/10.1007/BF02192855.
[65] M. Varadi, S. Anyango, M. Deshpande, S. Nair, C. Natassia, G. Yordanova, D. Yuan, O. Stroe, G. Wood, A. Laydon, A. Zídek, T. Green, K. Tunyasuvunakool, S. Petersen, J. Jumper, E. Clancy, R. Green, A. Vora, M. Lutfi, M. Figurnov, A. Cowie, N. Hobbs, P. Kohli, G. Kleywegt, E. Birney, D. Hassabis, S. Velankar, AlphaFold Protein Structure Database: massively expanding the structural coverage of protein-sequence space with high-accuracy models, Nucleic Acids Res. 50 (2022) D439–D444, https://doi.org/10.1093/NAR/GKAB1061.
[66] D. Kozakov, D.R. Hall, B. Xia, K.A. Porter, D. Padhorny, C. Yueh, D. Beglov, S. Vajda, The ClusPro web server for protein-protein docking, Nat. Protoc. 12 (2017) 255–278, https://doi.org/10.1038/NPROT.2016.169.
[67] M.F. Lensink, G. Brysbaert, T. Mauri, N. Nadzirin, S. Velankar, R.A.G. Chaleil, T. Clarence, P.A. Bates, R. Kong, B. Liu, G. Yang, M. Liu, H. Shi, X. Lu, S. Chang, R. S. Roy, F. Quadir, J. Liu, J. Cheng, A. Antoniak, C. Czaplewski, A. Giełdoń, M. Kogut, A.G. Lipska, A. Liwo, E.A. Lubecka, M. Maszota-Zieleniak, A. K. Sieradzan, R. Ślusarz, P.A. Wesołowski, K. Zięba, C.A. Del Carpio Muñoz, E. Ichiishi, A. Harmalkar, J.J. Gray, A.M.J.J. Bonvin, F. Ambrosetti, R. Vargas Honorato, Z. Jandova, B. Jiménez-García, P.I. Koukos, S. Van Keulen, C.W. Van Noort, M. Réau, J. Roel-Touris, S. Kotelnikov, D. Padhorny, K.A. Porter, A. Alekseenko, M. Ignatov, I. Desta, R. Ashizawa, Z. Sun, U. Ghani, N. Hashemi, S. Vajda, D. Kozakov, M. Rosell, L.A. Rodríguez-Lumbreras, J. Fernandez-Recio, A. Karczynska, S. Grudinin, Y. Yan, H. Li, P. Lin, S.Y. Huang, C. Christoffer, G. Terashi, J. Verburgt, D. Sarkar, T. Aderinwale, X. Wang, D. Kihara, T. Nakamura, Y. Hanazono, R. Gowthaman, J.D. Guest, R. Yin, G. Taherzadeh, B. G. Pierce, D. Barradas-Bautista, Z. Cao, L. Cavallo, R. Oliva, Y. Sun, S. Zhu, Y. Shen, T. Park, H. Woo, J. Yang, S. Kwon, J. Won, C. Seok, Y. Kiyota, S. Kobayashi, Y. Harada, M. Takeda-Shitaka, P.J. Kundrotas, A. Singh, I.A. Vakser, J. Dapkūnas, K. Olechnovič, Č. Venclovas, R. Duan, L. Qiu, X. Xu, S. Zhang, X. Zou, S.J. Wodak, Prediction of protein assemblies, the next frontier: the CASP14-CAPRI experiment, Proteins 89 (2021) 1800–1823, https://doi.org/10.1002/PROT.26222.
[68] B. Rizzuti, F. Grande, Virtual screening in drug discovery: a precious tool for a still-demanding challenge, in: Protein Homeostasis Diseases: Mechanisms and Novel Therapies, 2020, pp. 309–327, https://doi.org/10.1016/B978-0-12-819132-3.00014-2.
[69] G. Weng, E. Wang, Z. Wang, H. Liu, F. Zhu, D. Li, T. Hou, HawkDock: a web server to predict and analyze the protein-protein complex based on computational docking and MM/GBSA, Nucleic Acids Res. 47 (2019) W322–W330, https://doi.org/10.1093/NAR/GKZ397.
[70] H.D. Lewis, J. Liddle, J.E. Coote, S.J. Atkinson, M.D. Barker, B.D. Bax, K.L. Bicker, R.P. Bingham, M. Campbell, Y.H. Chen, C.W. Chung, P.D. Craggs, R.P. Davis, D. Eberhard, G. Joberty, K.E. Lind, K. Locke, C. Maller, K. Martinod, C. Patten, O. Polyakova, C.E. Rise, M. Rüdiger, R.J. Sheppard, D.J. Slade, P. Thomas, J. Thorpe, G. Yao, G. Drewes, D.D. Wagner, P.R. Thompson, R.K. Prinjha, D. M. Wilson, Inhibition of PAD4 activity is sufficient to disrupt mouse and human NET formation, Nat. Chem. Biol. 3 (11) (2015) 189–191, https://doi.org/10.1038/nchembio.1735.
[71] S.C. Stadler, C.T. Vincent, V.D. Fedorov, A. Patsialou, B.D. Cherrington, J. J. Wakshlag, S. Mohanan, B.M. Zee, X. Zhang, B.A. Garcia, J.S. Condeelis, A.M. C. Brown, S.A. Coonrod, C.D. Allis, Dysregulation of PAD4-mediated citrullination of nuclear GSK3β activates TGF-β signaling and induces epithelialto-mesenchymal transition in breast cancer cells, Proc. Natl. Acad. Sci. U. S. A. 110 (2013) 11851–11856, https://doi.org/10.1073/PNAS.1308362110/SUPPL_FILE/PNAS.201308362SI.PDF.
[72] Y. Zhang, Y. Yang, X. Hu, Z. Wang, L. Li, P. Chen, PADs in cancer: current and future, Biochim. Biophys. Acta Rev. Cancer 1875 (2021), https://doi.org/10.1016/J.BBCAN.2020.188492.
[73] Q. Duan, C. Pang, N. Chang, J. Zhang, W. Liu, Overexpression of PAD4 suppresses drug resistance of NSCLC cell lines to gefitinib through inhibiting Elk1-mediated epithelial-mesenchymal transition, Oncol. Rep. 36 (2016) 551–558, https://doi.org/10.3892/OR.2016.4780.
[74] A.E. Yuzhalin, A.N. Gordon-Weeks, M.L. Tognoli, K. Jones, B. Markelc, R. Konietzny, R. Fischer, A. Muth, E. O'Neill, P.R. Thompson, P.J. Venables, B. M. Kessler, S.Y. Lim, R.J. Muschel, Colorectal cancer liver metastatic growth depends on PAD4-driven citrullination of the extracellular matrix, Nat. Commun. 1 (9) (2018) 1–15, https://doi.org/10.1038/s41467-018-07306-7.
[75] D.E. Otzen, D.M.S. Lundvig, R. Wimmer, L.H. Nielsen, J.R. Pedersen, P.H. Jensen, p25alpha is flexible but natively folded and binds tubulin with oligomeric stoichiometry, Protein Sci. 14 (2005) 1396–1409, https://doi.org/10.1110/PS.041285605.
[76] L. Saelices, C.V. Galmozzi, F.J. Florencio, M.I. Muro-Pastor, J.L. Neira, The inactivating factor of glutamine synthetase IF17 is an intrinsically disordered protein, which folds upon binding to its target, Biochemistry 50 (2011) 9767–9778, https://doi.org/10.1021/BI2009272.
[77] J.L. Neira, F.J. Florencio, M.I. Muro-Pastor, The isolated, twenty-three-residue-long, N-terminal region of the glutamine synthetase inactivating factor binds to its target, Biophys. Chem. 228 (2017) 1–9, https://doi.org/10.1016/J.BPC.2017.05.017.
[78] B.G. Pierce, K. Wiehe, H. Hwang, B.H. Kim, T. Vreven, Z. Weng, ZDOCK server: interactive docking prediction of protein-protein complexes and symmetric multimers, Bioinformatics 30 (2014) 1771–1773, https://doi.org/10.1093/BIOINFORMATICS/BTU097.
[79] C. Manegold, Current advancements in hard-to-treat cancers, Am. J. Cancer 4 (2005) 105–113, https://doi.org/10.2165/00024669-200504020-00004/METRICS.
[80] K. Singh, K.A. Batich, P.Y. Wen, A.C. Tan, S.J. Bagley, M. Lim, M. Platten, H. Colman, D.M. Ashley, S.M. Chang, R. Rahman, E. Galanis, A. Mansouri, V. K. Puduvalli, D.A. Reardon, S. Sahebjam, J.H. Sampson, J. Simes, D.A. Berry, G. Zadeh, T.F. Cloughesy, M.P. Mehta, S. Piantadosi, M. Weller, A.B. Heimberger, M. Khasraw, Designing clinical trials for combination immunotherapy: a framework for glioblastoma, Clin. Cancer Res. 28 (2022) 593, https://doi.org/10.1158/1078-0432.CCR-21-2681.
[81] S.A. Artene, C. Tuţă, A. Dragoi, O. Alexandru, P. Stefana Oana, D.E. Tache, M. M. Dănciulescu, M.V. Boldeanu, C.A. Siloşi, A. Dricu, Current and emerging EGFR therapies for glioblastoma, J. Immunoass. Immunochem. 39 (2018) 1–11, https://doi.org/10.1080/15321819.2017.1411816.
[82] J.J. Adashek, F. Janku, R. Kurzrock, Signed in blood: circulating tumor DNA in cancer diagnosis, treatment and screening, Cancers (Basel) 13 (2021), https://doi.org/10.3390/CANCERS13143600.
[83] K. Rai, K.C. Akdemir, L.N. Kwong, P. Fiziev, C.J. Wu, E.Z. Keung, S. Sharma, N. S. Samant, M. Williams, J.B. Axelrad, A. Shah, D. Yang, E.A. Grimm, M.C. Barton, D.R. Milton, T.P. Heffernan, J.W. Horner, S. Ekmekcioglu, A.J. Lazar, J. Ernst, L. Chin, Dual roles of RNF2 in melanoma progression, Cancer Discov. 5 (2015) 1327, https://doi.org/10.1158/2159-8290.CD-15-0493.
[84] D. Zhu, Y. Zhang, S. Wang, Histone citrullination: a new target for tumors, Mol. Cancer 20 (2021) 1–17, https://doi.org/10.1186/S12943-021-01373-Z/FIGURES/2.
[85] A. Bosch, K. Panoutsopoulou, J.M. Corominas, R. Gimeno, G. Moreno-Bueno, J. Martín-Caballero, S. Morales, T. Lobato, C. Martínez-Romero, E.F. Farias, X. Mayol, A. Cano, I. Hernández-Muñoz, A. Bosch, K. Panoutsopoulou, J. M. Corominas, R. Gimeno, G. Moreno-Bueno, J. Martín-Caballero, S. Morales, T. Lobato, C. Martínez-Romero, E.F. Farias, X. Mayol, A. Cano, I. Hernández-Muñoz, The Polycomb group protein RING1B is overexpressed in ductal breast carcinoma and is required to sustain FAK steady state levels in breast cancer epithelial cells, Oncotarget 5 (2014) 2065–2076, https://doi.org/10.18632/ONCOTARGET.1779.